AFRL-RY-WP-TR-2010-1215

DATA COMPRESSION WITH APPLICATION TO GEO-LOCATION

William W. Perkins

Louisiana State University
Department of Electrical and Computer Engineering

AUGUST 2010
Final Report

AIR FORCE RESEARCH LABORATORY
SENSORS DIRECTORATE
WRIGHT-PATTERSON AIR FORCE BASE, OH 45433-7320
AIR FORCE MATERIEL COMMAND
UNITED STATES AIR FORCE

NOTICE AND SIGNATURE PAGE

Using Government drawings, specifications, or other data included in this document for any purpose other than Government procurement does not in any way obligate the U.S. Government. The fact that the Government formulated or supplied the drawings, specifications, or other data does not license the holder or any other person or corporation; or convey any rights or permission to manufacture, use, or sell any patented invention that may relate to them.

This report was cleared for public release by the Wright-Patterson Public Affairs Office and is available to the general public, including foreign nationals. Copies may be obtained from the Defense Technical Information Center (DTIC) (http://www.dtic.mil).

AFRL-RY-WP-TR-2010-1215 HAS BEEN REVIEWED AND IS APPROVED FOR PUBLICATION IN ACCORDANCE WITH ASSIGNED DISTRIBUTION STATEMENT.

*//Signature//

NIVIA COLON-DIAZ, Electronics Engineer
Integrated RF Sensor Technology Branch

//Signature//

KEITH W. LOREE, Chief (Ashley Schmitt, Acting Chief)
Integrated RF Sensor Technology Branch
RF Sensors Division
Sensors Directorate

//Signature//

For TRACY W. JOHNSTON, Chief
RF Sensors Division
Sensors Directorate

This report is published in the interest of scientific and technical information exchange, and its publication does not constitute the Government's approval or disapproval of its ideas or findings.

*Disseminated copies will show "//Signature//" stamped or typed above the signature blocks.

REPORT DOCUMENTATION PAGE

Form Approved
OMB No. 0704-0188

1. REPORT DATE *(DD-MM-YY)*	2. REPORT TYPE	3. DATES COVERED *(From - To)*
August 2010	Final	08 September 2006 – 31 August 2010

4. TITLE AND SUBTITLE
DATA COMPRESSION WITH APPLICATION TO GEO-LOCATION

5a. CONTRACT NUMBER

5b. GRANT NUMBER
FA8650-05-D-1912-0007

5c. PROGRAM ELEMENT NUMBER
62204F

6. AUTHOR(S)
William W. Perkins

5d. PROJECT NUMBER
7622

5e. TASK NUMBER
11

5f. WORK UNIT NUMBER
7622110P

7. PERFORMING ORGANIZATION NAME(S) AND ADDRESS(ES)
Louisiana State University
Department of Electrical and Computer Engineering
Baton Rouge, LA 70803

8. PERFORMING ORGANIZATION REPORT NUMBER

9. SPONSORING/MONITORING AGENCY NAME(S) AND ADDRESS(ES)
Air Force Research Laboratory
Sensors Directorate
Wright-Patterson Air Force Base, OH 45433-7320
Air Force Materiel Command
United States Air Force

10. SPONSORING/MONITORING AGENCY ACRONYM(S)
AFRL/RYRR

11. SPONSORING/MONITORING AGENCY REPORT NUMBER(S)
AFRL-RY-WP-TR-2010-1215

12. DISTRIBUTION/AVAILABILITY STATEMENT
Approved for public release; distribution unlimited.

13. SUPPLEMENTARY NOTES
PAO Case Number: 88ABW 2007-1747; Clearance Date: 27 July 2007. This is a thesis submitted in partial fulfillment of the requirements for the Degree of Master of Science in Electrical Engineering in the Department of Electrical and Computer Engineering at Louisiana State University. This document contains color.

14. ABSTRACT
A common way to locate an emitter within a wireless sensor network requires the estimation of time-difference-of-arrival (TDOA) parameters using data collected by a set of spatially separated sensors. Compressing the data that is shared among the sensors can provide tremendous savings in terms of the energy and transmission latency. Traditional MSE and perceptual based data compression schemes fail to accurately capture the effects of compression on the TDOA estimation task; therefore, it is necessary to investigate compression algorithms suitable for TDOA parameter estimation.

This thesis explores the effects of data compression on TDOA parameter estimation accuracy. The first part of this document investigates the decimation of band-limited communication signals which are oversampled to achieve high precision in the TDOA estimate. In the second part, we follow the work of [19-22] in implementing a Fisher Information-based subband encoding scheme, an approach that has been shown to provide better results than the traditional MSE-based approach. A pseudo-QMF filter bank [8] is implemented, which is computationally more efficient than wavelet packet filter banks, at the cost of relaxing perfect reconstruction conditions. Additionally, a suboptimal bit allocation algorithm is developed which further lessens the sensor resource requirements for compression.

15. SUBJECT TERMS

16. SECURITY CLASSIFICATION OF:			17. LIMITATION OF ABSTRACT:	18. NUMBER OF PAGES	19a. NAME OF RESPONSIBLE PERSON (Monitor)
a. REPORT	b. ABSTRACT	c. THIS PAGE			Nivia Colon-Diaz
Unclassified	Unclassified	Unclassified	SAR	72	19b. TELEPHONE NUMBER *(Include Area Code)* N/A

Standard Form 298 (Rev. 8-98)
Prescribed by ANSI Std. Z39-18

Table of Contents

List of Figures

List of Tables

In Loving Memory of Brianna Murphy

Acknowledgements

I would first like to thank Dr. Jorge Aravena. Without his guidance, this work would not have been possible. He has been a most excellent advisor and mentor, and I will be forever grateful for his efforts in helping me achieve my goal of pursuing a higher education.

I would like to thank my family, Alanna, and my friends for their support throughout these times. I would also like to thank Dr. Shuangqing Wei for his insightful discussions pertaining to communications engineering and information theory, many of the ideas from our discussions played a significant role in the development of this thesis. I would like to thank Dr. Mark Folwer for helping me to understand his work.

Finally, I would like to wish the best of luck to the many friends that I have made who are currently pursuing their master's degree or PhD.

Chapter 1

Introduction

1.1 Position and Velocity Estimation

Wireless location finding has emerged as an essential public safety feature in cellular networks due to a mandate issued by the FCC in 1996 [1]. The E911 mandate requires wireless service providers to deliver the accurate location of a 911 caller to emergency responders. In addition to its immediate EMS and military applications, there exists much potential in the commercial sector as well [1][2]. As the use of location sensitive applications becomes more prevalent, the demand for reliable, cost-effective passive location systems will subsequently grow [1][2].

A commonly used method for estimating the position of an emitter within a wireless sensor network requires the use of *time-difference-of-arrival* (*TDOA*) measurements [3][4]. The locus of points where the difference in distance to two sensors is proportional to the TDOA estimate obtained from the sensors is a hyperbola on which the emitter lies (Fig. 1.1). If the elevation of the emitter is known, at least 3 sensors are required to determine its position [5]. Including additional information from redundant sensors can help to improve the accuracy of the estimation. Similarly, the velocity of an emitter can be determined using *frequency-difference-of-arrival* (*FDOA*) information.

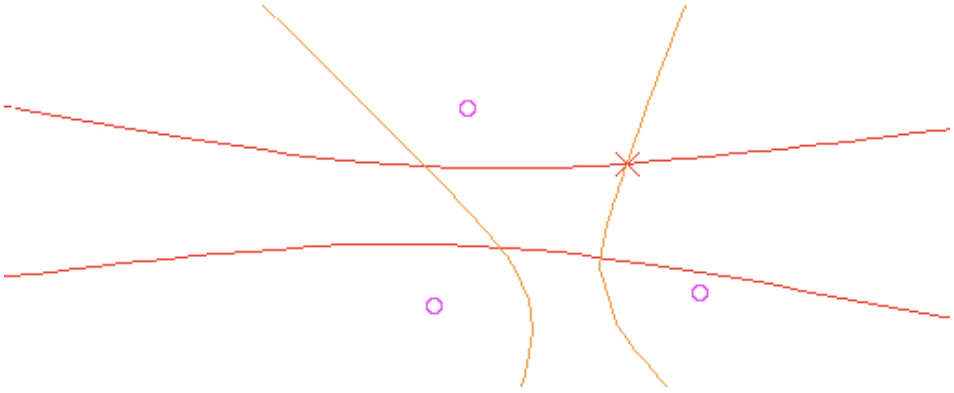

Figure 1.1 Passive location of emitter using TDOA estimates

1.2 The Data Compression Issue

In order to estimate TDOA or FDOA parameters, it is necessary for information to be shared between sensors. Sharing data among sensors can introduce significant network delays that may affect the performance of the location application. To minimize network latency and reduce power consumption by, possibly, mobile sensors, the data collected by each sensor should be compressed before it is transmitted to a neighboring sensor (Fig 1.2a) or a central fusion center (Fig 1.2b) for processing.

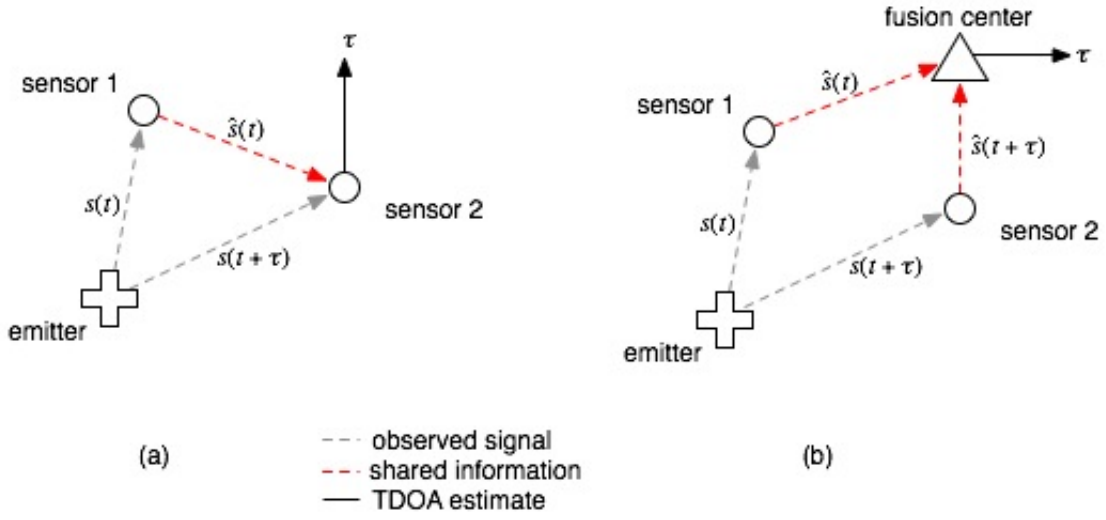

Figure 1.2 (a) distributed estimation (b) centralized estimation

In addition to noise introduced at each receiver, the combined decimation and quantization of the signal information will also contribute noise to TDOA estimate. Unlike traditional perceptual encoding schemes, the fidelity criterion of this particular application is the impact on the TDOA/FDOA parameter estimates.

1.3 Scope of Work

This thesis will outline the issues related with compressing data for the purpose of geo-location and will develop a tool which will aid in the design of compression algorithms for digital linearly modulated signals of the form:

$$v(t) = \sum_{n=-\infty}^{\infty} I_n g(t - nT) \qquad (1.1)$$

Where $\{I_n\}$ is a sequence of symbols, $g_T(t)$ is a transmission filter, and $v(t)$ is the continuous time complex envelope of the modulated signal. Examples of digital modulation techniques which are of the form in equation 1.1 include *pulse amplitude modulation* (PAM), *phase shift keying* (PSK), and *quadrature amplitude modulation* (QAM).

The developments in the remainder of this thesis do not include the effects of multipath or fading. Additionally, it is assumed that the sensors and fusion center have clocks which are perfectly synchronized, so the effects of clock jitter are also not included.

Chapter 2

Literature Review

2.1 Data Compression Overview

Data Compression or *Source Coding* is the process of removing unwanted redundancy from a signal while satisfying a fidelity criterion to reduce transmission bandwidth or space required for storage [6]. Some examples of popular perceptual [6] encoding schemes include the MPEG [6][7] and JPEG [6][7] standards.

A common lossy data compression algorithm structure consists of several stages as depicted in Fig. 2.1. First, the input is transformed to a domain suitable for encoding. The samples of the transformed signal are then selectively mapped to a smaller set of symbols, which require fewer bits to represent, through the process of quantization. The compressed data is then transmitted over a channel to a decoder which decodes the quantized sequence and restores the information to its original domain.

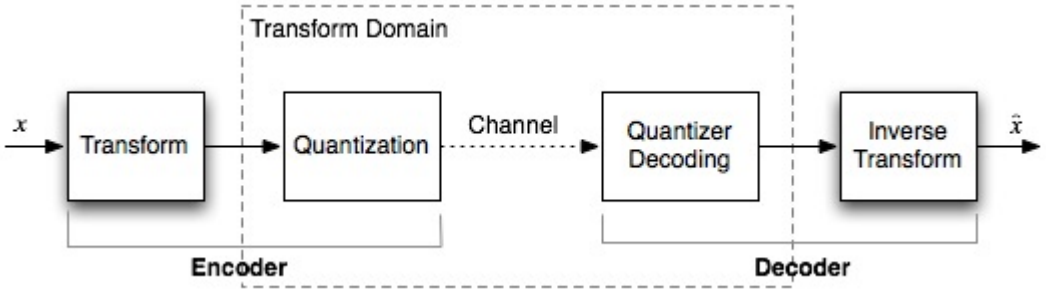

Figure 2.1 A common lossy data compression algorithm structure

The majority of existing lossy compression schemes are designed for multimedia applications and, consequentially, use perceptual based measures to determine loss of fidelity. The focus of this thesis will be on the effects of lossy compression on TDOA/FDOA estimation.

2.2 Transform Coding

It is common in data compression schemes to transform a signal into a domain that is more suitable for analysis or encoding. For example, in subband coding, a signal is decomposed into a number of frequency subbands (Fig. 2.2), each of which can be encoded independently (Fig 2.2). There exist many techniques for performing subband decomposition including quadrature-mirror filtering (QMF) and polyphase decomposition [7]. Two special cases of these methods are presented: the wavelet packet transform [7] and the pseudo-quadrature mirror filter bank [8].

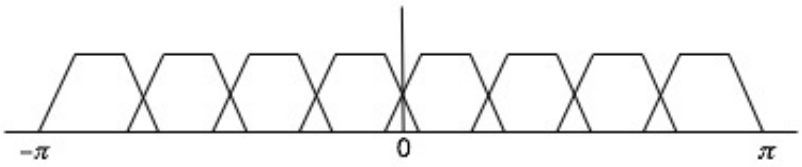

Figure 2.2 Subband Decomposition

The wavelet packet transform (WPT) is a cascade of quadrature-mirror filter banks and can take on any dyadic tree structure (Fig 2.3). Because QMF banks satisfy the perfect reconstruction perfect reconstruction conditions, the input to a WPT analysis filter bank can be perfectly reconstructed by a companion synthesis filter bank. Aliasing which is introduced by overlapping from adjacent frequency bands will be completely cancelled. Although the WPT allows for perfect reconstruction, due to its recursive nature, it is not the most computationally efficient structure.

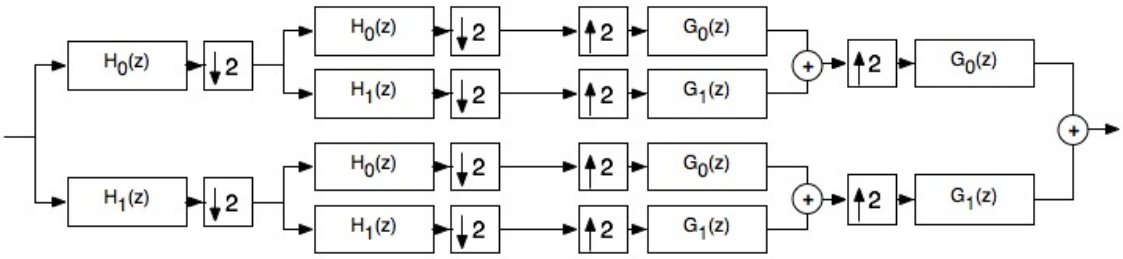

Figure 2.3 Wavelet Packet Decomposition

If the perfect reconstruction conditions are relaxed, a more efficient structure can be implemented such as the pseudo-quadrature mirror filter bank (PQF)[8]. The pseudo-quadrature mirror filter bank is a cosine-modulated filter bank which is designed to minimize, but not eliminate, aliasing between adjacent frequency subbands. Section 2.6 provides a more detailed description of the filter bank and a brief analysis of its performance. In general, the order of a near-perfect reconstruction filter is much smaller than that of a perfect reconstruction filter with the same transition band slope. Additionally, the number of operations required by a polyphase filter bank is less than that of a recursive filter bank.

2.3 Quantization

Quantization is the process of mapping the outputs of an information source, $\mathbf{x}$, to a representation sequence, $\hat{\mathbf{x}}$, which requires fewer bits to describe. The function which defines the mapping is called a quantizer [9][10]. In scalar quantization, each single-source output is quantized into a number of levels and the levels are encoded into a binary sequence [9][10]. If we are dealing with an analog source, each output is a real number. A scalar quantizer, $Q(\cdot)$, partitions $\Re$ into N disjoint subsets, $\Re_i, 1 \le i \le N$ [11]. Corresponding to each subset, $\Re_i$, is a representation point, $\hat{x}_i$ (Fig. 2.4).

Figure 2.4 Scalar quantization of $\Re$

If the source output at time k, x_k, belongs to $\Re_i$, it is then represented by $\hat{x}_i$ [9].

$$Q(x) = \hat{x}_i \text{ for all } x \in \Re_i \qquad (2.1)$$

The quantized symbol at time k, $\hat{x}_k$, is then encoded as a binary sequence and transmitted. Since there are N quantization levels, the number of bits required to transmit each source output is $R = \log_2 N$.

Since quantization provides a many-to-one mapping (i.e. $\Re_i \rightarrow \hat{x}_i$), the original source symbol, x_k, can not be obtained from its quantized version, $\hat{x}_k$. The distance between a source output at time k, x_k, and its quantized version, $\hat{x}_k$, can be expressed as the function $d(x_k, \hat{x}_k)$. A commonly used distortion measure is the *squared-error* [6][9] [11][12]:

$$d(x_k, \hat{x}_k) = (x_k - \hat{x}_k)^2 \qquad (2.2)$$

If $d(x_k, \hat{x}_k)$ is the distortion measure per single source output, then distortion between a sequence of n outputs, $\mathbf{X}^n$, and the corresponding quantized values, $\hat{\mathbf{X}}^n$,is the average of the distortion between the individual outputs:

$$d(\mathbf{X}^n, \hat{\mathbf{X}}^n) = \frac{1}{n}\sum_{k=1}^{n} d(x_k, \hat{x}_k) \qquad (2.3)$$

Equation 2.3 assumes that the position of the error in the sequence is unimportant [9]. Since the source output is a random process, $d(\mathbf{X}^n, \hat{\mathbf{X}}^n)$ is a random variable. The distortion for the source is defined as the expected value of the random variable $d(\mathbf{X}^n, \hat{\mathbf{X}}^n)$.

$$D = E[d(\mathbf{X}^n, \hat{\mathbf{X}}^n)] = \frac{1}{n}\sum_{k=1}^{n} E[d(x_k, \hat{x}_k)] = E[d(x_k, \hat{x}_k)] \qquad (2.4)$$

Where the final equality in equation 2.4 holds under the assumption that the source output is a stationary random process [12].

The distortion, D, can be expressed as a function of the rate, R [9][11]. In general, D is monotonically decreasing in R [9][10][11][12]. A well known result in rate-distortion theory [10][12] is that the distortion-rate function, $D(R)$, of a discrete-time, continuous-amplitude, memoryless source with zero-mean and finite variance, σ_x^2, (with respect to the mean-squared-error distortion measure) is upper bounded by:

$$D(R) \le \sigma_x^2 2^{-2R} \qquad (2.5)$$

Where equality holds when the source outputs are Gaussian with variance σ_x^2 [12]. The limit in 2.5 can be approached asymptotically using very complex encoders and decoders [9].

The simplest scalar quantizer is the uniform quantizer, which has regions, $\Re_i$, of equal length, Δ, (with the exception of $\Re_1$ and $\Re_N$). Uniform quantization is optimal when the probability density function (PDF) of the source output is uniform. If the PDF of the source output is known and is not uniform, an optimal quantizer can be designed through use of an algorithm which iteratively determines the boundaries of the partition regions [13].

For the scenario of a wireless sensor network, we use uniform scalar quantization due to its ease of implementation and our lack of knowledge of source statistics. For a finite amplitude signal in additive noise, the partition length, Δ, is given by [19]:

$$\Delta = \frac{\sqrt{A^2 + \sigma^2}}{2^{b-1} - \frac{1}{2}} \qquad (2.6)$$

Where A is the peak amplitude of the signal, σ^2 is the variance of additive noise, and b is the number of bits allocated for quantization.

2.4 Bit Allocation

In a transform coding scheme, it is often required to encode segments of a signal independently, for example, in subband encoding, each frequency subband is separately encoded. Given a single rate constraint and a set of subbands to be individually quantized, the problem of determining an appropriate way to allocate bits arises.

As mentioned in the previous section, the distortion introduced by quantization can be expressed as a function of the rate, $D(R)$. For an M-channel subband encoder, each subband will have its own rate-distortion function, $D_i(R), 1 \le i \le M$. When the distortion measure is additive, the total distortion can be computed as the sum of the distortion of the individual subbands. Given a set of independent rate-distortion functions, $D_i(R)$, the task of finding a bit allocation vector, $B = \{b_i \ge 0 | i \in 1,2,\cdots,M\}$, which minimizes the total distortion, using less than R bits, is defined as:

$$\min_B \left\{ \sum_{i=1}^{M} D_i(b_i) \right\} \text{ subjec} \qquad \text{t to: } \left\{ \sum_{i=1}^{M} b_i \le R \right\} \qquad (2.6)$$

When a signal is stationary and its statistics are known a priori, a model can be used to determine a bit allocation vector, B, which will be optimal on average. If the signal is highly non-stationary

or its statistics are not known, an operational algorithm can be used to calculate an optimal bit allocation for *each* block which is quantized. Determining the bit allocation requires solving the constrained optimization problem in equation 2.6, which may not be computationally feasible for a wireless sensor to perform on each quantization block. An efficient Lagrange multiplier based technique [14] has been implemented to solve the integer optimization problem off-line (see Appendix A). It is assumed that a central fusion center will observe a portion on an intercepted signal and calculate a bit allocation vector, *B*, which will then be sent to the sensors. Performing the bit allocation at the fusion center will reduce the resources required by each sensor without significantly affecting the overall geo-location task.

If the rate-distortion functions are not convex, or do not contain a point which meets the required budget, then the Lagrange optimization method will not provide an optimal solution [6]. When the Lagrange multiplier method is inadequate, the allocation can be formulated as a deterministic dynamic programming problem. Although dynamic programming can provide a better solution, it requires significantly more resources to implement and may not be feasible in real-time applications.

2.5 TDOA and FDOA Parameter Estimation

In order to develop a distortion measure which is appropriate for geo-location, it is important to examine the TDOA and FDOA estimation process. The TDOA parameter is determined by observing data received by a pair of physically separated sensors (Fig 2.5a) and searching for the time offset of a hypothesized common signal. Likewise, the FDOA parameter can be found by determining the frequency offset between the signals received at the sensors (Fig. 2.5b). A common way to perform the estimation process is through the use of cross-correlation [15].

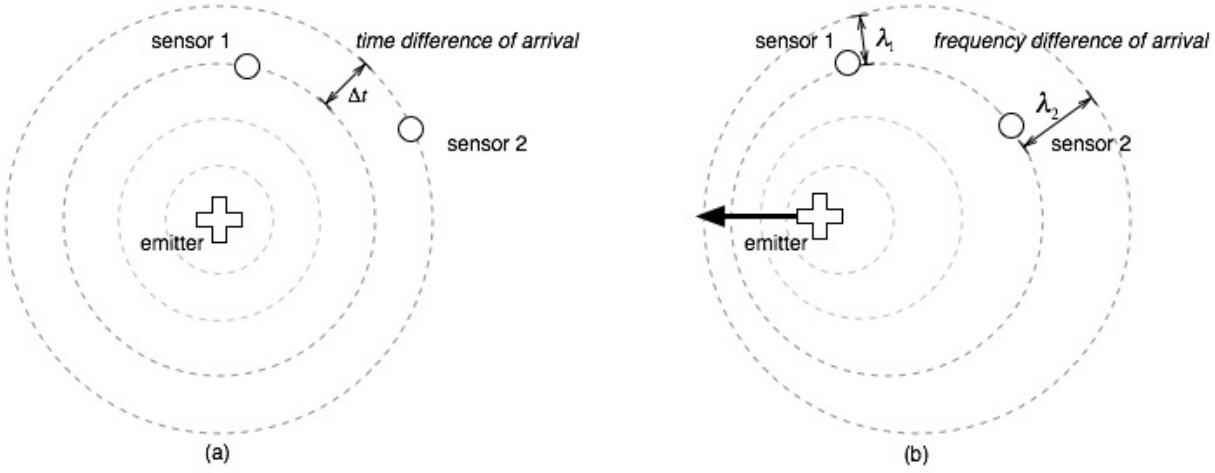

Figure 2.5 (a) stationary emitter (b) mobile emitter in wireless sensor network

Let $x_1(t)$ denote the signal observed by sensor 1 and $x_2(t)$ the signal observed by sensor 2. Let both signals contain a common component $s(t)$ and a white Gaussian noise component, $n_i(t)$,

which is assumed to be independent at each sensor.

$$x_1(t) = s(t)e^{j2\pi f_1 t} + n_1(t) \qquad (2.7)$$
$$x_2(t) = s(t-D)e^{j2\pi f_2 t} + n_2(t) \qquad (2.8)$$

The *complex ambiguity function* (CAF) [15][4] is defined as:

$$A(\tau, f) = \int_0^T x_1(t)x_2^*(t+\tau)e^{-j2\pi ft}dt \qquad (2.9)$$

Notice that the CAF is the cross-correlation of the signals observed by the two sensors, modulated by a term *f*. The time lag, τ, and frequency shift, *f*, parameters are to be searched simultaneously for values that maximize $|A(\tau, f)|$. The combined TDOA/FDOA estimation process can be expressed as:

$$\max_{\tau, f} |A(\tau, f)| \qquad (2.10)$$

Assuming that there are no hidden periodicities in the signals $x_1(t)$ and $x_2(t)$, and the parameters τ and *f* remain constant within the integration time *T*; the ambiguity function will peak as $\tau \to D$ and $f \to f_1 - f_2$, creating a unique "correlation lobe" (Fig. 2.6).

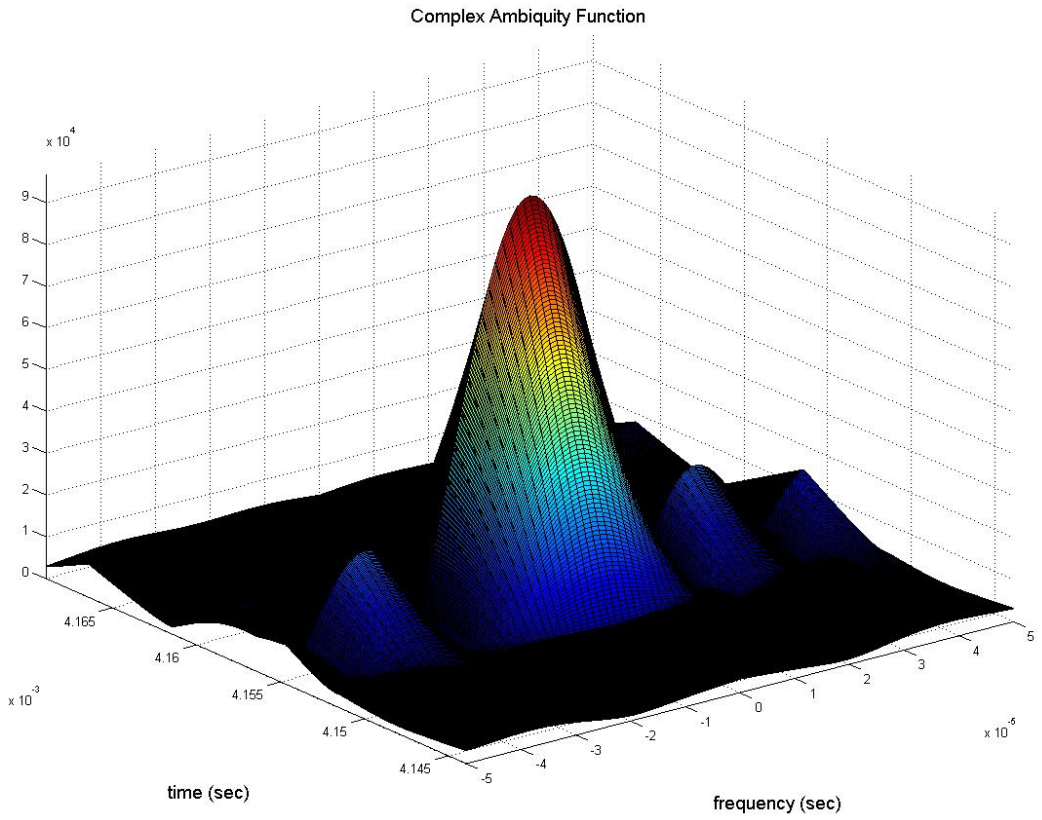

Figure 2.6 Complex Ambiguity Function

Given that $s(t)$ is aperiodic, the CAF should possess a unique, clearly defined maximum. When the signals $x_i(t)$ contain additive noise $n_i(t)$, the peak location of the CAF will be perturbed. It has been shown [4][15][16] that the TDOA and FDOA estimates are unbiased and have a variance that achieves the Cramer-Rao bound when any of several reasonable techniques is used to locate the apparent peak. When the additive noise, $n_i(t)$, is white and Gaussian, the Cramer-Rao lower bounds for TDOA and FDOA estimation are given as [15][16]:

$$\sigma_{TDOA} \geq \frac{1}{\beta}\frac{1}{\sqrt{BT\gamma}} \qquad \text{where} \quad \beta = 2\pi\left[\frac{\int f^2|S(f)|^2\,df}{\int |S(f)|^2\,df}\right]^{1/2} \tag{2.11}$$

$$\sigma_{FDOA} \geq \frac{1}{T_e}\frac{1}{\sqrt{BT\gamma}} \qquad \text{where} \quad T_e = 2\pi\left[\frac{\int t^2|s(t)|^2\,dt}{\int |s(t)|^2\,dt}\right]^{1/2} \tag{2.12}$$

Where $|S(f)|^2$ is the power spectrum density of the source signal $s(t)$, B is the noise bandwidth at the receiver, T is the integration time, β is termed *rms radian frequency*, T_e is termed *rms integration time*, and γ is the effective input signal-to-noise ratio (SNR)[4][15]:

$$\frac{1}{\gamma} = \frac{1}{2}\left[\frac{1}{\gamma_1} + \frac{1}{\gamma_2} + \frac{1}{\gamma_1\gamma_2}\right] \tag{2.13}$$

Where γ_1 is the SNR at sensor 1 and γ_2 is the SNR at sensor 2. In order to accurately perform the estimation, the integration time-bandwidth product must be large, $BT >> 1$. A small effective SNR, γ, will degrade the accuracy of the estimate; however, the accuracy can be further improved by increasing the receiver bandwidth, B, or observation time, T.

In order to improve the asymptotic performance of an unbiased estimator, we wish to minimize the Cramer-Rao lower bound or, equivalently, maximize its reciprocal, the Fisher Information, J [17].

$$\sigma^2{}_{TDOA} \geq J^{-1} \tag{2.14}$$

Lossy compression of the observed signal, $x_i(t)$, will change its probability density function (PDF), which will, consequently, affect the value of the Fisher Information (FI). Let $J(x;\tau)$ denote the FI of the observed signal with respect to the TDOA parameter, τ, and $J(\hat{x};\tau)$ denote the FI of the compressed signal. Our goal is to compress the observed signal in such a way that the difference in Fisher Information is minimized:

$$\min_{\hat{x}}\{J(x;\tau) - J(\hat{x};\tau)\} \tag{2.14}$$

Since $J(x;\tau) \geq J(\hat{x};\tau)$, for any compression scheme, the goal is [19]:

$$\max_{\hat{x}}\{J(\hat{x};\tau)\} \tag{2.15}$$

The Fisher Information for TDOA estimation when the two observed signals contain additive white Gausian noise can be expressed as [15][16]:

$$J(x;\tau) = BT\gamma \frac{\int_{-\infty}^{\infty} f^2 |S(f)|^2 df}{\int_{-\infty}^{\infty} |S(f)|^2 df} \tag{2.16}$$

When the SNR at the two sensors is large, i.e. $\gamma_1 >> 1, \gamma_2 >> 1$, the third term in equation 2.13 is negligible and the effective SNR, γ, is approximately:

$$\gamma = \frac{2\gamma_1\gamma_2}{\gamma_1 + \gamma_2} \tag{2.17}$$

The SNR for the i^{th} sensor is defined as:

$$\gamma_i = \frac{\int_{-\infty}^{\infty} |S(f)|^2 df}{\sigma_i^2} \tag{2.18}$$

Where σ_i^2 is the variance of the zero-mean additive white Gaussian noise at the i^{th} sensor. Using equation 2.18, the effective SNR, γ, can be rewritten as:

$$\gamma = \frac{2\int_{-\infty}^{\infty} |S(f)|^2 df}{\sigma_1^2 + \sigma_2^2} \tag{2.19}$$

Now, substituting the expression for the effective SNR (Eq. 2.19) into equation 2.16, the Fisher Information can then be expressed as:

$$J(x;\tau) = 2BT \frac{\int_{-\infty}^{\infty} f^2 |S(f)|^2 df}{\sigma_1^2 + \sigma_2^2} \tag{2.20}$$

Focusing on the compression task at sensor *i*, we wish to compress the intercepted signal, $x_i(t)$, to maximize equation 2.20. For a fixed time-bandwidth product, *BT*, the term which we wish to maximize at sensor *i* is proportional to:

$$\frac{1}{\sigma_i^2}\int_{-\infty}^{\infty} f^2 |S(f)|^2 df \tag{2.21}$$

This approach has been used in previous works [18][19][20][22] in which the source signal, $s(t)$, is a frequency modulated (FM) signal. Their works indicate that the FI-based approach provides better results than using standard MSE distortion criteria when compressing signals for TDOA and FDOA estimation. For the remainder of this thesis, we will follow the work of [19][21][22] in developing a model for the Fisher Information which characterizes the effects of lossy compression on the TDOA estimation task.

As discussed in section 2.3, quantization introduces noise. The signal, $\hat{x}_i[k]$, resulting from quantization of samples of the intercepted signal, $x_i(t)$, can be expressed as:

$$\hat{x}_i[k] = s[k] + n_i[k] + e[k] \tag{2.22}$$

Where $s[k]$ is the sampled source signal at time k, $n_i[k]$ is the sensor noise, and $e[k]$ is the quantization noise. Following the work of [19][22], we will model the quantization noise, e, as white, uniformly distributed, zero mean, and independent of the sensor noise, n_i, when the samples are quantized using multiple bits [19][22]. For multi-bit quantization, if $\text{var}\{e\} << \text{var}\{n_i\}$, then the sum of the random variables, e and n_i, will result in a random variable that is approximately Gaussian, with a variance that is the sum of the variances of the two random variables [19]. Including the effects of quantization noise (for the multi-bit case) into equation 2.21, we can then express the quantity which we are trying to maximize as:

$$\frac{\int_{-\infty}^{\infty} f^2 |S(f)|^2 df}{\sigma_i^2 + q^2} \tag{2.23}$$

Where q^2 is the variance of the quantization noise, which we model by [19]:

$$q^2 = \sqrt{3}\pi/2 \, \sigma^2 2^{-2b} \tag{2.24}$$

Where σ^2 is the variance of the intercepted signal, and b is the number of bits used for quantization. As done in [19][21][22], we will use the Discrete Fourier Transform (DFT) of the intercepted signal, $x_i(t)$, to evaluate the Fisher Information for the multi-bit quantization case [19] (the superscript "m" in $\tilde{J}^{(m)}$ signifies multi-bit).

$$\tilde{J}^{(m)}(X_i[n]) = \frac{2\pi^2 \sum_{n=-N/2}^{N/2-1} n^2 |X_i[n]|^2}{N\sigma_i^2 + q_n^2} \tag{2.25}$$

Where $X_i[n], -N/2 \le n \le N/2 - 1$ are the DFT coefficients of the samples of the signal $x_i(t)$; σ_i^2 is the variance of the sensor noise, $n_i(t)$ (scaled by N as a result of the DFT [19]); and q_n^2 is the variance of the quantization noise for the n^{th} sample. Notice that the Fisher Information (Eq. 2.20) is dependent on the power spectrum density of the *source* signal, $s(t)$. For the FI

evaluation (Eq. 2.25) we are using the DFT of the *observed* signal, $x_i(t)$, which contains both the source signal, $s(t)$, and the sensor noise, $n_i(t)$; therefore, the expression which we are evaluating (eq. 2.25) is approximately the Fisher Information.

Since the Fisher Information is proportional to the integral of the quadratically weighted PSD (Eq, 2.21), the choice of the DFT as the transform for analysis allows us examine the contribution of frequency components to the overall FI; therefore, we can selectively quantize frequency subbands to maximize the total FI.

For the case of quantization to a single bit, the assumption that the variance of the sensor noise is large than the variance of the quantization noise no longer holds. We use the numerically computed FI given in [19] for quantization using a single bit:

$$\tilde{J}^{(1)}(X_1[n]) = \frac{4}{\pi N\sigma^2} n^2 \left| \mathrm{Im}^2\{X_i[n]\} \exp\left(-\frac{2}{N\sigma^2}\mathrm{Re}^2\{X_i[n]\}\right) \times \frac{1}{1-erf^2(\mathrm{Re}\{X_i[n]\}/(\sqrt{N}\sigma))} \right| + \frac{4}{\pi N\sigma^2} n^2 \left| \mathrm{Re}^2\{X_i[n]\} \exp\left(-\frac{2}{N\sigma^2}\mathrm{Im}^2\{X_i[n]\}\right) \times \frac{1}{1-erf^2(\mathrm{Im}\{X_i[n]\}/(\sqrt{N}\sigma))} \right| \tag{2.26}$$

Where $X_i[n], -N/2 \le n \le N/2 - 1$ are the DFT coefficients of the samples of the signal $x_i(t)$, and the superscript "1" in $\tilde{J}^{(1)}$ signifies single-bit quantization.

In [21] the authors use the Discrete Fourier Transform to evaluate the Fisher Information of an intercepted signal, while using the Wavelet Packet Transform to transform the data for encoding. Similar to their approach, we will use the DFT to evaluate the FI, and employ the Pseudo-QMF bank to transform the data for encoding.

2.6 Pseudo-QMF Filter Bank

The pseudo-quadrature mirror filter (PQF) bank [8] is a cosine-modulated filter bank which is designed to cancel aliasing between adjacent frequency subbands. Aliasing introduced by non-adjacent subbands is comparable to stopband attenuation. Due to its highly symmetric structure, the PQF can be implemented much more efficiently than the ordinary wavelet packet transform [7].

The difficulty of designing a pseudo-QMF bank lies in creating a single low-pass FIR prototype filter from which the rest of the filter bank can be constructed [7][23][24]. Once the prototype is obtained, its impulse response coefficients, $h(n)$, are modulated by a cosine term to created each subband filter. The k^{th} bandpass filter, $H_k(n)$, of an M channel analysis filter bank is obtained by [8]:

$$H_k(n) = h(n)\cos\left(\frac{(2k+1)}{2M}n - \frac{\pi}{4}\right) \tag{2.27a}$$

Similarly, the synthesis filters, $G_k(n), 1 \le k \le M$, are obtained by [8]:

$$G_k(n) = h(n)\cos\left(\frac{(2k+1)}{2M}n + \frac{\pi}{4}\right) \qquad (2.27b)$$

The operation of performing M filter convolutions with a window size of N requires $M \times N$ multiplications and $M \times (N-1)$ additions. The implementation of the PQF requires $2M^2 + N$ multiplications and $2M^2 - 3M + N$ additions when the number of subbands is a power of 2 and the prototype filter has length of 16 times the number of subbands [8]. Figure 2.7 demonstrates the computational savings of the pseudo-QMF filter bank, when using the previously mentioned optimization [8], versus performing M separate filter convolutions.

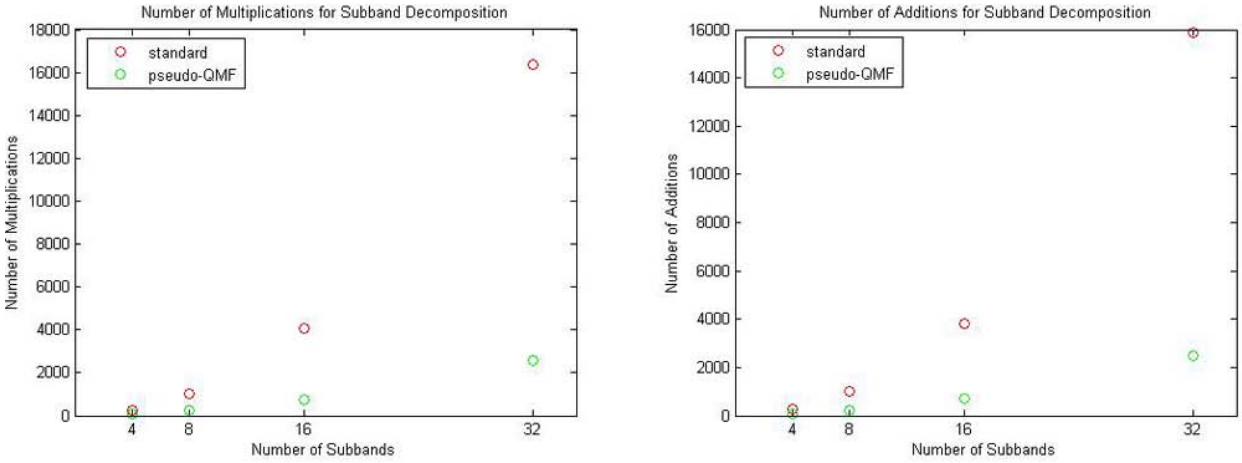

Figure 2.7 Analysis filter bank (a) multiplications (b) additions

Table 2.1 Analysis filterbank (a) multiplications (b) additions

Analysis Filterbank Multiplications		
subbands	**standard**	**PQF**
4	256 96	
8	1024 256	
16	4096 768	
32	16384 2560	

Analysis Filterbank Additions		
subbands	**standard**	**PQF**
4	252 84	
8	1016 232	
16	3840 720	
32	15872 2464	

The filter bank is built from a single prototype filter which is designed to satisfy near-perfect reconstruction conditions within a certain tolerance [7]. The design of such a prototype filter generally requires solving a nonlinear constrained optimization problem [24]. For our simulations, we used the prototype filter coefficients specified in the MPEG audio standard [25].

2.7 Spectral Characteristics of Digital Linearly Modulated Signals

In order to develop an efficient bit allocation scheme for subband coding, it is important to determine the spectral content of the digitally modulated signal. Consider a random information sequence $\{I_n\}$ which is to be transmitted over a channel. A modulator maps the digital information into analog waveforms that match the characteristics of the channel [10]. We will consider the class of memoryless linear modulation methods with the following base-band representation [10]:

$$v(t) = \sum_{n=-\infty}^{\infty} I_n g_T(t - nT) \qquad (2.28)$$

Where $\{I_n\}$ is a set of digital symbols, $g_T(t)$ is a pulse-shaping filter (Fig 2.8), and the pulse duration is *T*.

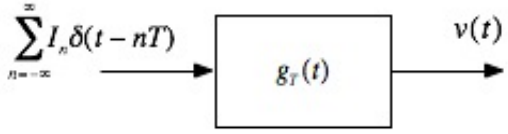

Figure 2.8 Digital sequence shaped by transmission filter

Examples of modulation methods belong to this class include *pulse amplitude modulation, phase-shift keying*, and *quadrature amplitude modulation* [9][10]. Assuming that $\{I_n\}$ is a wide-sense stationary process with mean, μ_i, and variance, σ_i^2, the power spectrum density (PSD) of the modulated signal (in baseband form) can be expressed as [10]:

$$\phi_{vv}(f) = \frac{\sigma_i^2}{T}\left|G(f)\right|^2 + \frac{\mu_i}{T}\sum_{m=-\infty}^{\infty}\left|G(\tfrac{m}{T})\right|^2 \delta(f - \tfrac{m}{T}) \qquad (2.29)$$

Where $\left|G(f)\right|^2$ is the PSD of the pulse shaping filter, $g_T(t)$. When the information symbols $\{I_n\}$ are equally likely and symmetrically distributed in the complex plane [10], $\mu_i = 0$, and the discrete part of equation 2.29 vanishes:

$$\phi_{vv}(f) = \frac{\sigma_i^2}{T}\left|G(f)\right|^2 \qquad (2.30)$$

This implies that under the given conditions, the PSD of the baseband signal is simply a scaled version of the PSD of the pulse shaping filter, $\left|G(f)\right|^2$.

It is assumed that the sensors we will be using are provided with the carrier frequency of the signal, so that we can remove the carrier component and encode the complex envelope of the signal. Given the complex envelope of a digitally modulated signal of the form in equation 2.28, assuming that the sequence $\{I_n\}$ is a zero-mean stationary random process, if we capture a sufficiently long portion of the signal and observe its spectrum, we can compute the Fisher Information and determine an appropriate bit allocation. The bit allocation will be effective for

the remaining duration of the signal so long as the pulse shaping filter or symbol rate, $1/T$, does not change.

Chapter 3

The Effects of Decimation

3.1 Motivation for decimation

In order to accurately perform the TDOA estimation process, it is necessary to sample the observed continuous-time signal at a very high rate. The cross-correlation of two discrete-time signals will yield a discrete sequence; therefore, when searching for the peak of the cross-correlated signals, the precision of the estimate will be limited to integer multiples of the sampling period (assuming interpolation is not used).

Consider a signal which is sampled at a rate of 20 MHz, providing a resolution of 50 ns. If we quantize the discrete-time signal using only one bit per sample, the overall rate will be 20 Mbps, which is infeasible for many real-time systems. Additionally, if we oversample band-limited communication signals, it is possible to resample at the Nyquist rate without introducing significant distortion. In an effort to further reduce the overall code rate, we will explore the use of decimation to reduce the sampling rate used for transmission.

3.2 Overview of decimation

When the continuous-time, baseband signal is sampled at a rate of $F_s = 1/T_s$, its resulting spectrum will be periodic with a period of F_s. We will consider the region centered at the origin, confined to the interval, $f \in [-F_s/2, F_s/2]$, or equivalently, $\omega \in [-\pi, \pi]$ (Fig. 3.1).

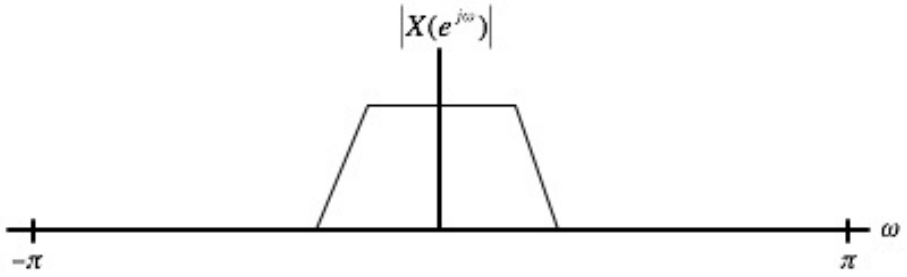

Figure 3.1 Spectra of a discrete-time signal

The down-sampling of a signal will effectively "expand" [25] its spectra. If the rate is reduced below the Nyquist rate, it may be necessary to pass the signal through a low-pass filter, $H_d(z)$, prior to down-sampling in order to avoid aliasing of the folded spectrum, (Fig. 3.2).

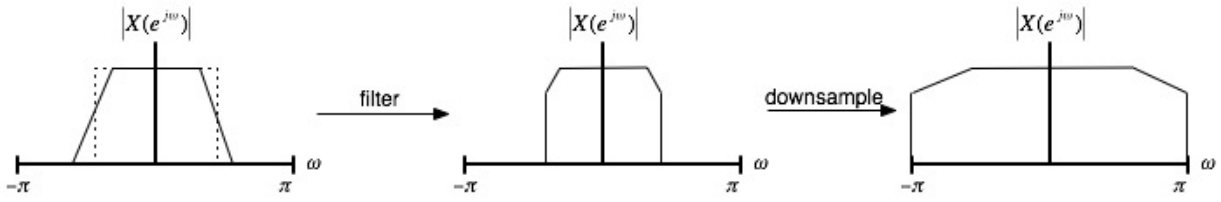

Figure 3.2 The process of decimation

At the receiver end, we wish to restore the signal to its original sampling rate before cross-correlation in order to regain fine precision in the TDOA estimate. Up-sampling the signal will "compress" [25] its spectra, causing images of the signal to be introduced into the upper end of the spectrum. These images can be removed by passing the up-sampled signal through an interpolation filter, $H_u(z)$, (Fig. 3.3).

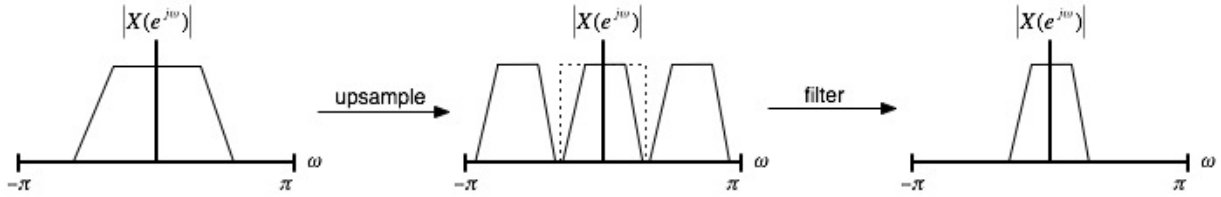

Figure 3.3 The process of interpolation

A decimation/interpolation codec which was implemented for the geo-location scenario is depicted in figure 3.4. The discrete-time baseband signal, $x(n)$, is first passed through a low-order FIR filter, $H_d(z)$, and is then downsampled by a factor of L. When the decimation factor, L, is very large, the decimation process is divided into two stages. The decimated signal is then transmitted over a channel to a receiver which up-samples the signal by the factor, L, and passes it through an interpolation filter, $H_u(z)$. The reconstructed signal, $\hat{x}(n)$, is then used to perform the TDOA estimation.

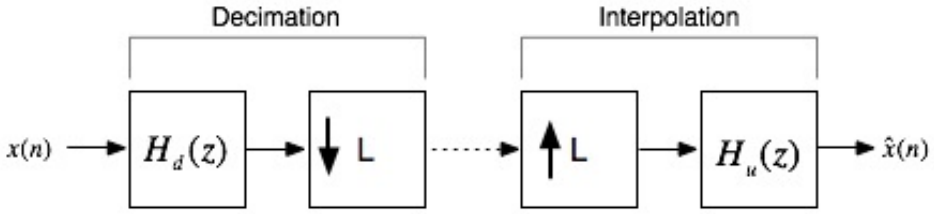

Figure 3.4 Structure of a decimation/interpolation codec

3.3 Experimental Results

In our experiments, we used two different pulse-shaping filters: a rectangle (Fig. 3.5a), and a raised-cosine (Fig. 3.5b).

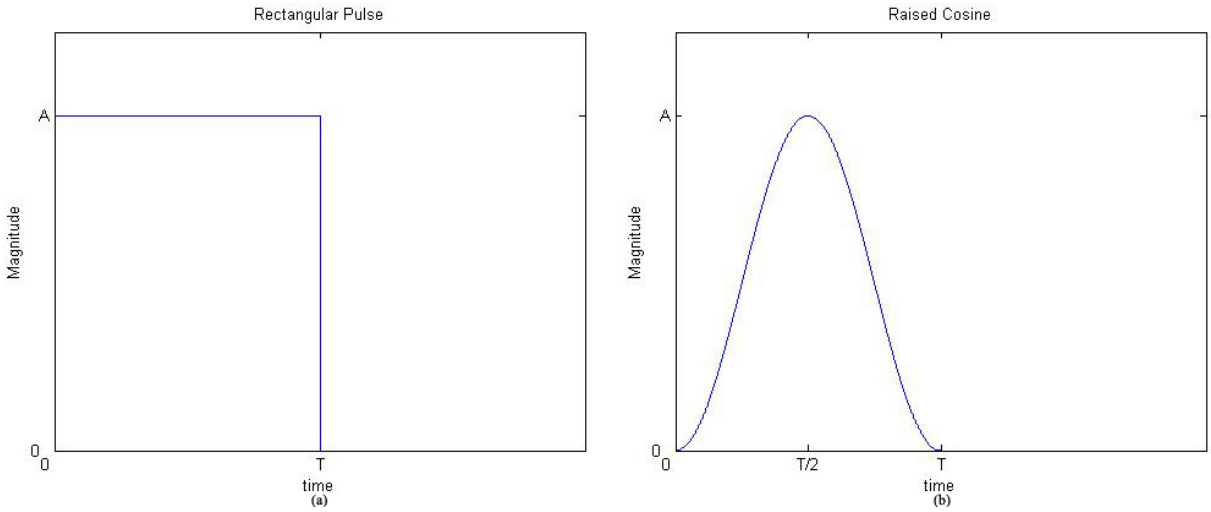

Figure 3.5 (a) rectangular pulse (b) raised-cosine pulse

We will first derive the power spectrum density of the linearly modulated signals using the two filters. The rectangular pulse is defined as:

$$g(t) = A, 0 \le t \le T \qquad (3.1)$$

Which has the power spectrum density (PSD):

$$|G(f)|^2 = (AT)^2 \left(\frac{\sin \pi f T}{\pi f T} \right)^2 \qquad (3.2)$$

Using the result obtained in equation 2.30, we can express the PSD of the linearly modulated baseband signal as:

$$\phi(f) = \sigma_i^2 A^2 T \left(\frac{\sin \pi f T}{\pi f T} \right)^2 \qquad (3.3)$$

Let, $\tilde{\phi}(f)$, denote the PSD of the band-limited random process, sampled at the rate $F_s = 1/T_s$. The PSD of the sampled signal is then:

$$\tilde{\phi}(f) = \frac{1}{T_s^2} \sum_{n=-\infty}^{\infty} \phi(f - \tfrac{n}{T_s}) \qquad (3.4)$$

For our analysis, we will consider the spectrum on the interval $f \in [-F_s/2, F_s/2]$

$$\tilde{\phi}(f) = \frac{1}{T_s^2} \sigma_i^2 A^2 T \left(\frac{\sin \pi f T}{\pi f T} \right)^2, |f| \le F_S/2 \qquad (3.5)$$

Figure 3.6 compares the theoretically obtained PSD (Eq. 3.5) with the PSD of an observed signal where the pulse duration is 5ns, and it is sampled at a rate of 20MHz. The symbols, $\{I_n\}$, are i.i.d., uniformly distributed with zero-mean.

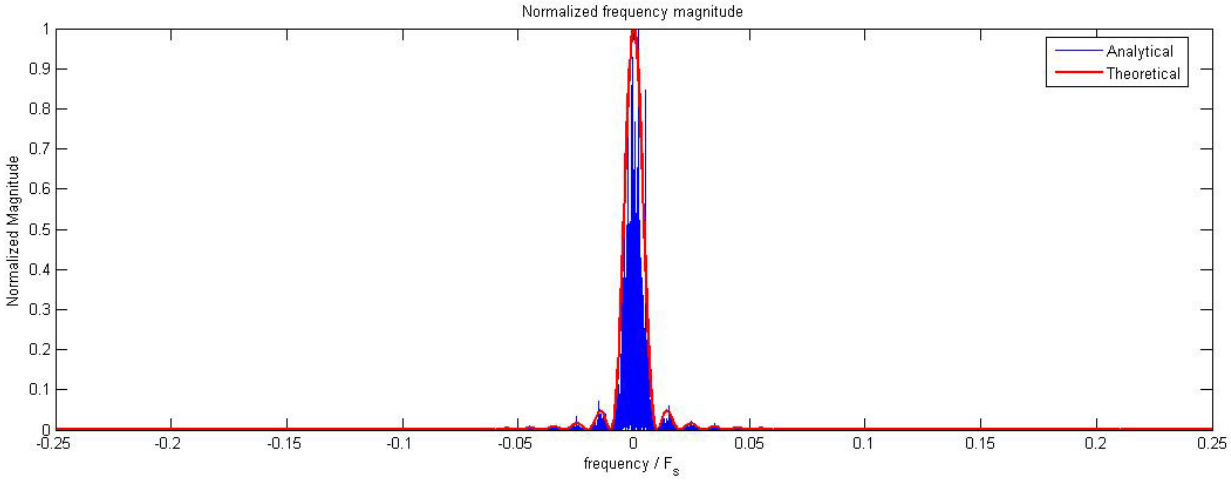

Figure 3.6 PSD of rectangular pulse-shaped signal with 5 ns period, sampled at 20 MHz

The PSD of the rectangular pulse decays proportional to $1/f^2$, as indicated in equation 3.5. Upon observation of the PSD (Fig. 3.6), it is apparent that its magnitude is very small in the range $|f| > 0.05$, which means that the signal can be significantly decimated without removing a large amount of energy. In order to better illustrate the cumulative distribution of power in the spectrum of a continuous-time rectangular pulse, we have numerically integrated its PSD (Fig. 3.7).

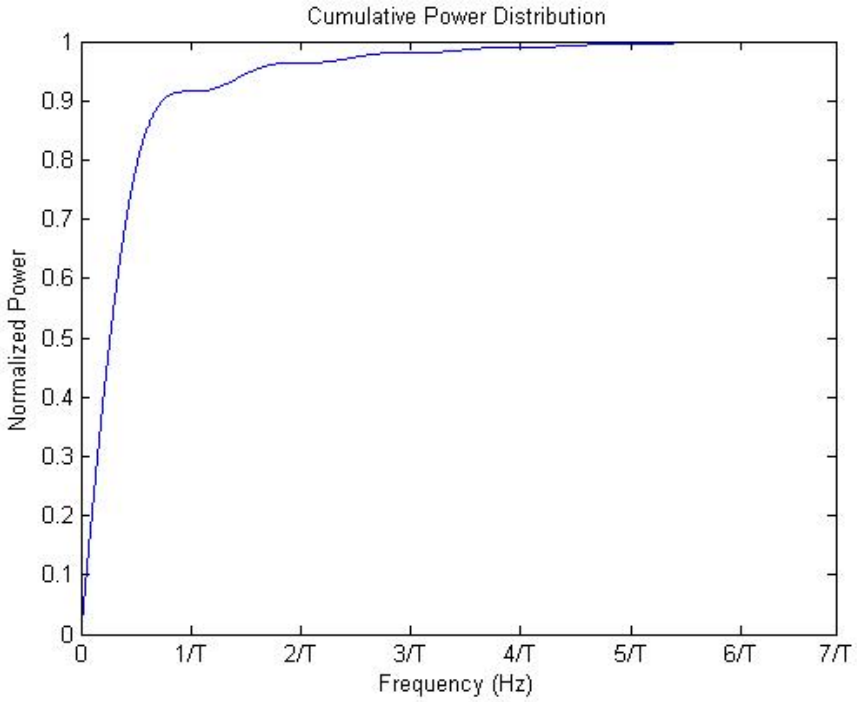

Figure 3.7 Cumulative power distribution of a rectangular pulse

Notice that the cumulative power grows at a large rate for low frequencies ($f < \frac{1}{T}$), and at high frequencies, the cumulative power approaches 1 asymptotically.

To illustrate the effects of decimation on the spectrum of the signal, we decimate an observed signal by a factor of 50, effectively removing all but the central lobe (Fig. 3.8).

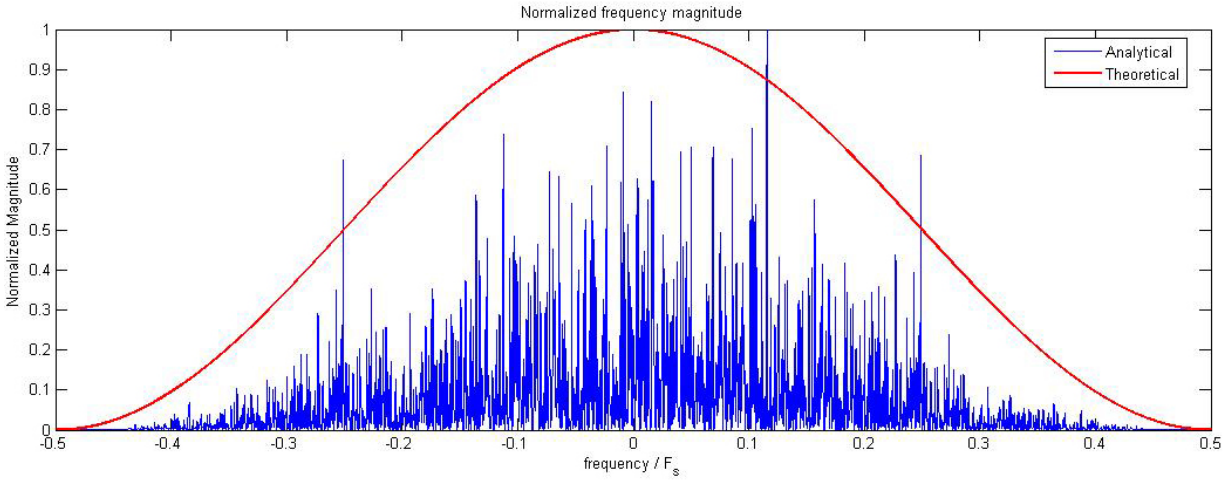

Figure 3.8 PSD of decimated signal

After the signal has been transmitted to a fusion center, prior to cross-correlation, the signal is upsampled to its original sampling rate and is then interpolated. Figure 3.9 shows the spectrum of the interpolated signal which is used for TDOA estimation. Notice that the central lobe is slightly attenuated at its edges due to the non-ideal transition bands of the decimation and interpolation filters.

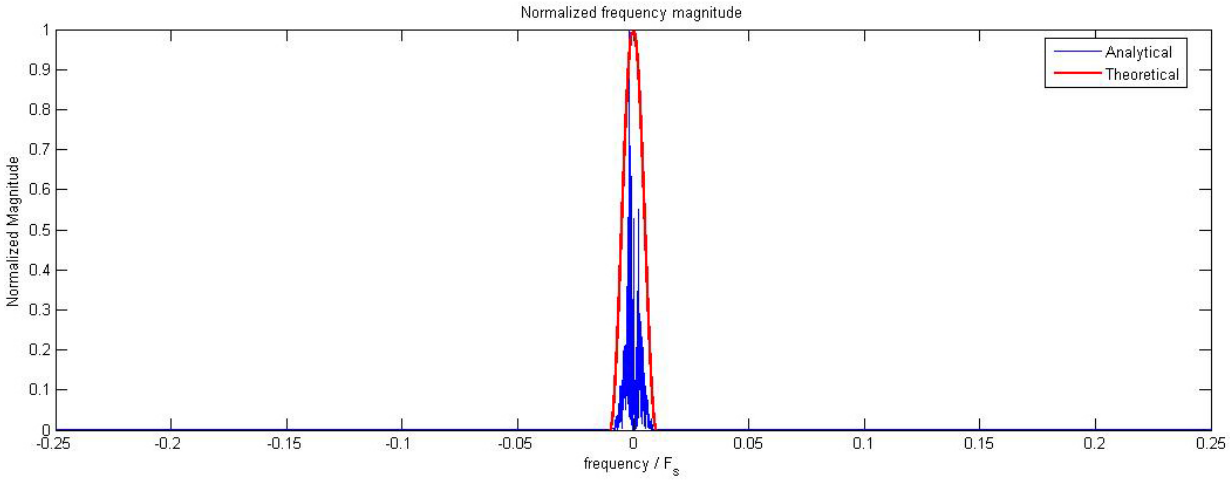

Figure 3.9 PSD of interpolated signal

The second pulse-shaping filter we experimented with is the raised-cosine, of the form:

$$g(t) = \frac{A}{2}\left[1 + \cos\frac{2\pi}{T}\left(t - \frac{T}{2}\right)\right], 0 \le t \le T \quad (3.6)$$

Which has a power spectrum density (PSD) defined as:

$$|G(f)|^2 = \left(\frac{AT}{2}\right)^2 \frac{\sin^2 \pi f T}{(\pi f T)^2 (1 - f^2 T^2)^2} \quad (3.7)$$

Using equation 2.30, we can express the PSD of the linearly modulated baseband signal as:

$$\phi(f) = \frac{\sigma_i^2 A^2}{4} \frac{\sin^2 \pi f T}{(\pi f)^2 (1 - f^2 T^2)^2} \quad (3.8)$$

The spectrum of the sampled signal, centered at $f = 0$ is:

$$\tilde{\phi}(f) = \frac{\sigma_i^2 A^2}{4T_s^2} \frac{\sin^2 \pi f T}{(\pi f)^2 (1 - f^2 T^2)^2}, |f| \le F_s/2 \quad (3.9)$$

Figure 3.10 compares the result from equation 3.9 to the PSD of an observed signal, shaped by a raised-cosine pulse with a duration of 5 ns, sampled at 20 MHz. The modulated symbols, $\{I_n\}$, are i.i.d., uniformly distributed, with zero-mean.

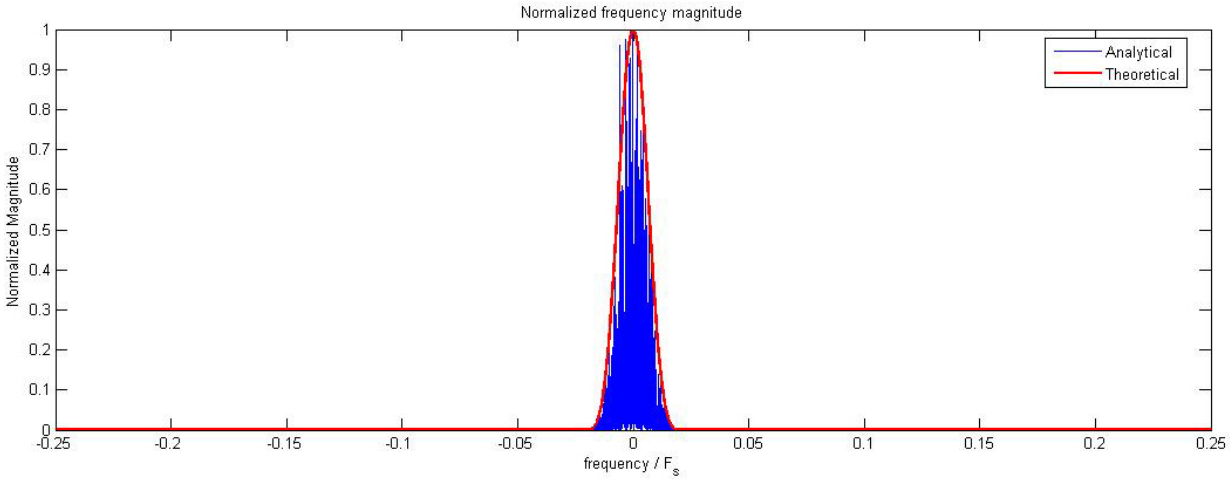

Figure 3.10 PSD of raised cosine pulse with 5 ns period, sampled at 20 MHz

Notice that the central lobe of the spectrum of the raised cosine is wider than central lobe of the sinc function (it does not have zeros at $f = -1/T, 1/T$). Also, the PSD of the raised cosine decays proportional to $1/f^6$. As figure 3.10 demonstrates, the magnitude of the side lobes is very small (not even visible in the graph). Figure 3.11 contains a plot of the cumulative power distribution of a raise-cosine pulse, similar to figure 3.7 for the rectangular pulse. Notice that the cumulative

power grows at a large rate for low frequencies ($f < \frac{2}{T}$), and at high frequencies, the cumulative power approaches 1 asymptotically.

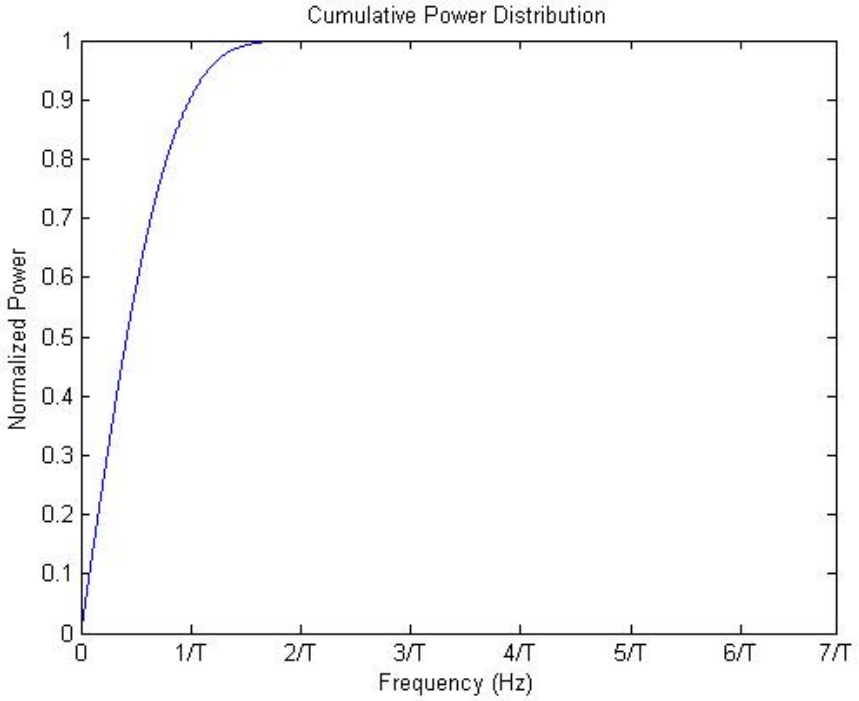

Figure 3.11 Cumulative power distribution of a rectangular pulse

To illustrate the effects of decimation on the spectrum of a raised-cosine shaped signal, we decimate an observed signal by a factor of 25, discarding all side lobes (Fig. 3.12).

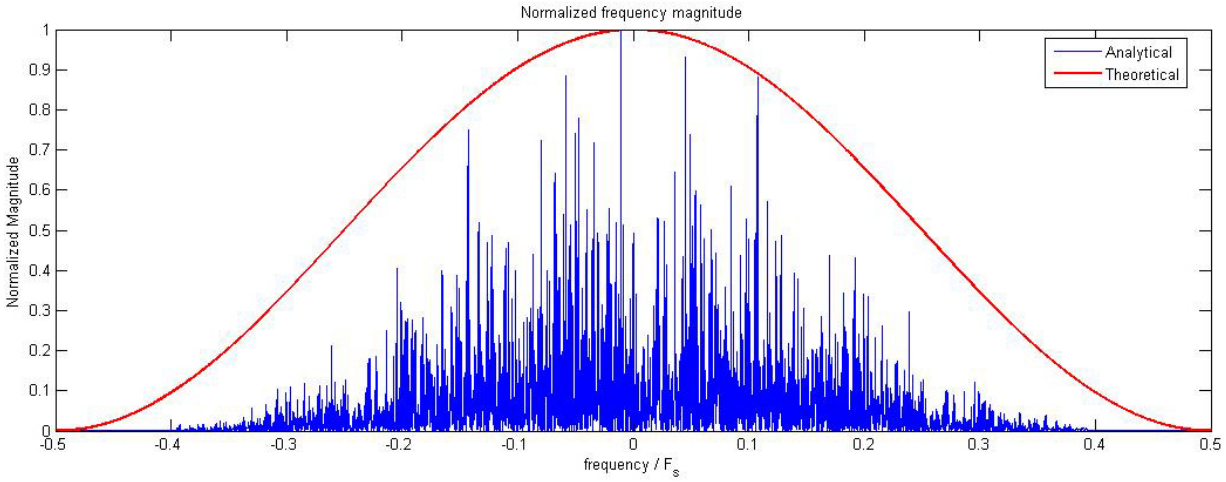

Figure 3.12 PSD of decimated signal

Figure 3.12 shows the PSD of the interpolated signal used for TDOA estimation. Notice that the PSD of the interpolated signal is not very different than the original signal, as the majority of the

power is contained in the central lobe. The central lobe is slightly attenuated at its edges due to the non-ideal transition bands of the decimation and interpolation filters.

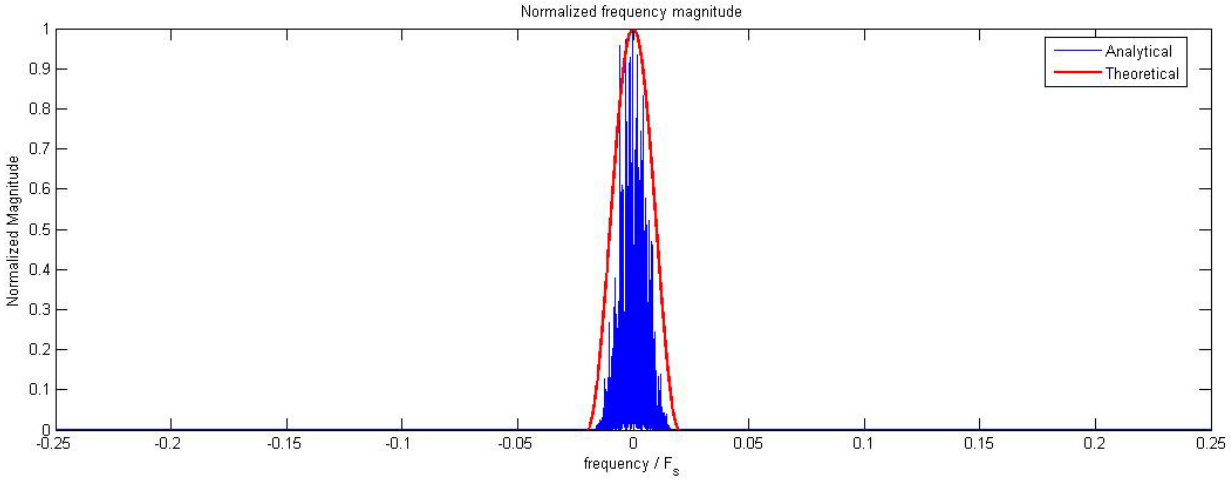

Figure 3.13 PSD of interpolated signal

We performed a series of experiments to investigate the effects of decimation on the TDOA estimation process. In the experiments, we used a fixed sampling rate of 20 MHz and generated signals with symbol rates up to 2.5 million symbols per second. The signals were comprised of a sequence of i.i.d., uniformly distributed symbols, randomly generated with zero-mean unit variance, and modulated using a pulse with duration, T.

The sequence length and symbol rate, $1/T$, were jointly chosen to produce signals with a duration on the order of 3 ms. To simulate centralized estimation (Fig. 1.2b), where two sensors share their signals with a fusion center, we decimated two signals by a factor, L, ranging from 2 to 48, and then interpolated by the same factor prior to cross-correlation. The resulting TDOA estimate was compared to an estimate obtained by cross-correlating the same signals without using decimation/interpolation. Similarly, to simulate distributed estimation (Fig 1.2a), we decimated and interpolated only one of the two signals.

Figures 3.14 and 3.15 show the variance of the TDOA estimation error obtained from performing the decimation experiment 100 times with a rectangular pulse-shaping filter. The results in figure 3.14 are for the centralized estimation case, figure 3.15 depicts the results of the distributed estimation case. In the graphs, the symbol rate, relative to the sampling rate is given in the units *samples per symbol*.

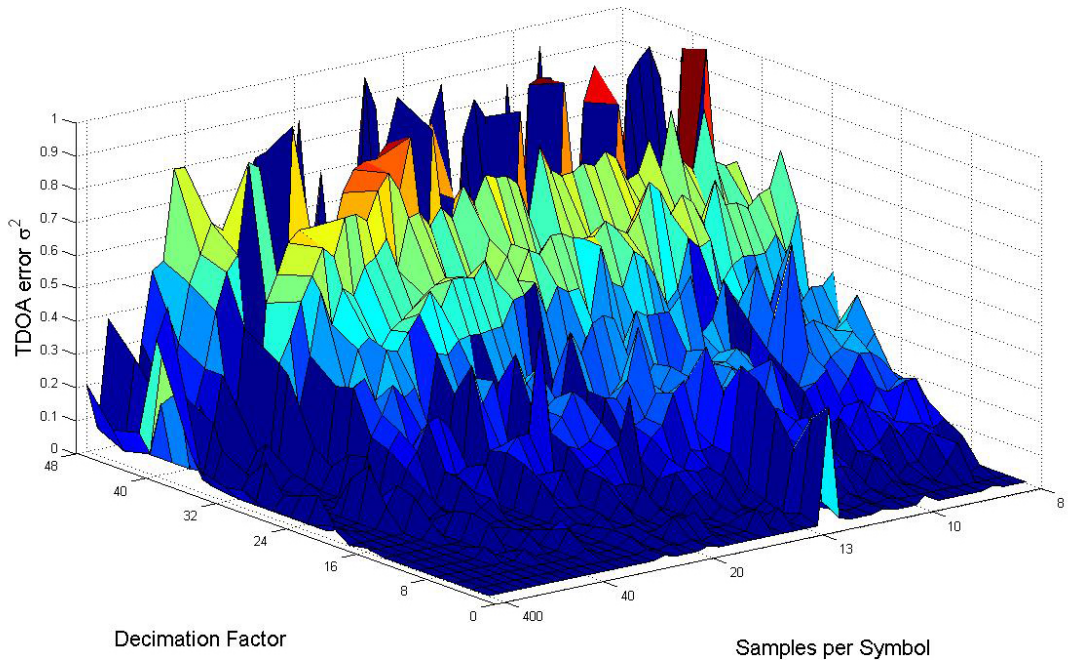

Figure 3.14 TDOA error as a function of symbol rate and decimation factor (rectangle, centralized)

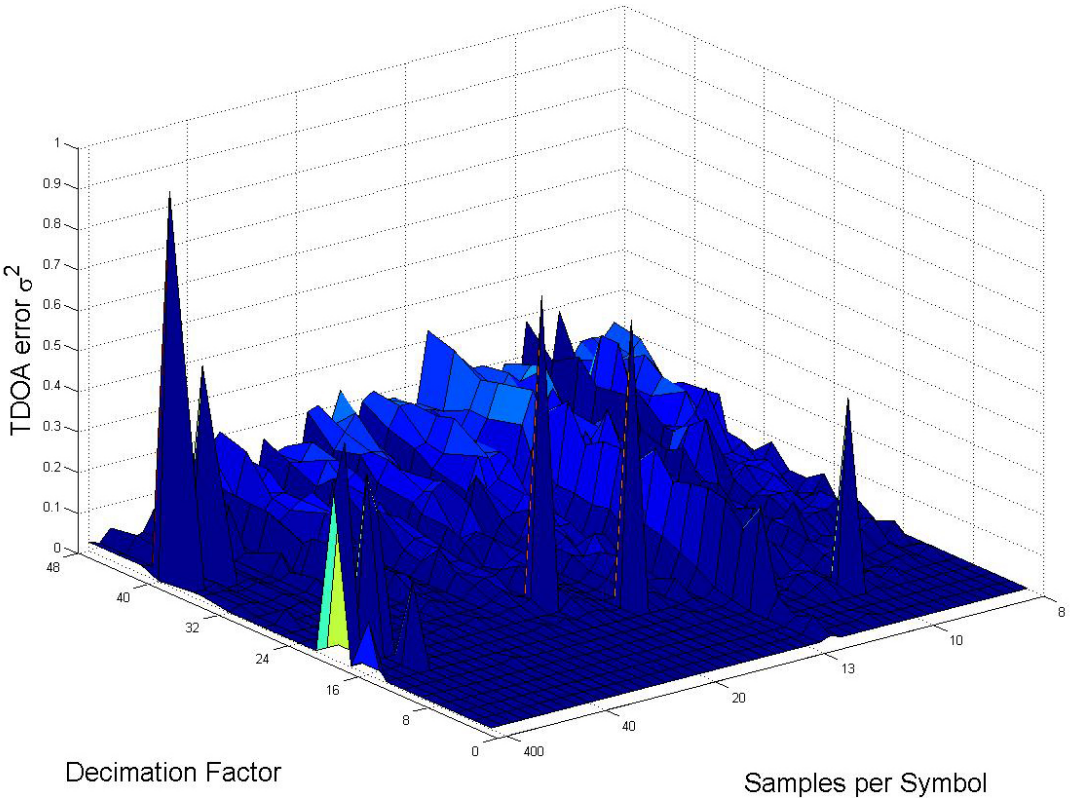

Figure 3.15 TDOA error as a function of symbol rate and decimation factor (rectangle, distributed)

In comparing figure 3.14 with figure 3.15, it is apparent that the TDOA estimation error is significantly less when only one of the two signals is decimated and interpolated. Additionally, in both cases, the TDOA error introduced by decimating signals with low symbols rates is minimal.

The same decimation experiments were also performed with signals which were shaped using a raised-cosine pulse. Figures 3.16 and 3.17 depict the results of the raised-cosine experiments. Once again, the TDOA error introduced by decimation in the distributed estimation scenario (Fig. 3.17) is significantly less than the error introduced in the centralized estimation scenario (Fig. 3.16).

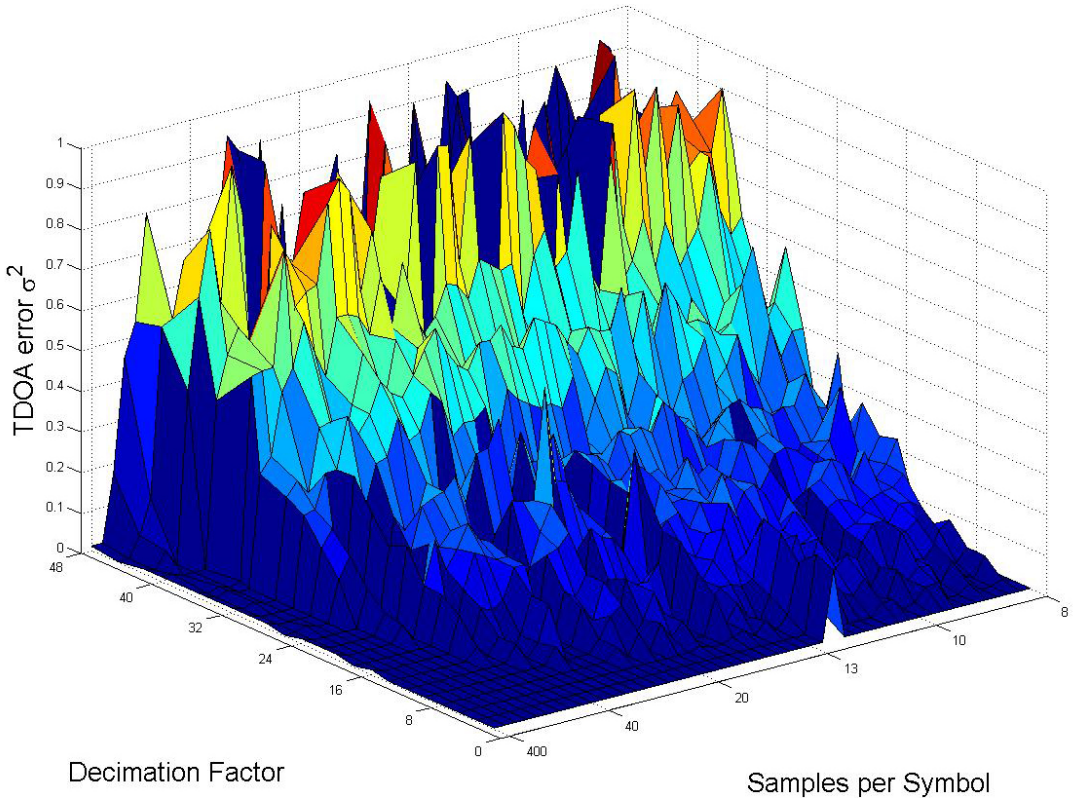

Figure 3.16 TDOA error as a function of symbol rate and decimation factor (raised-cosine, centralized)

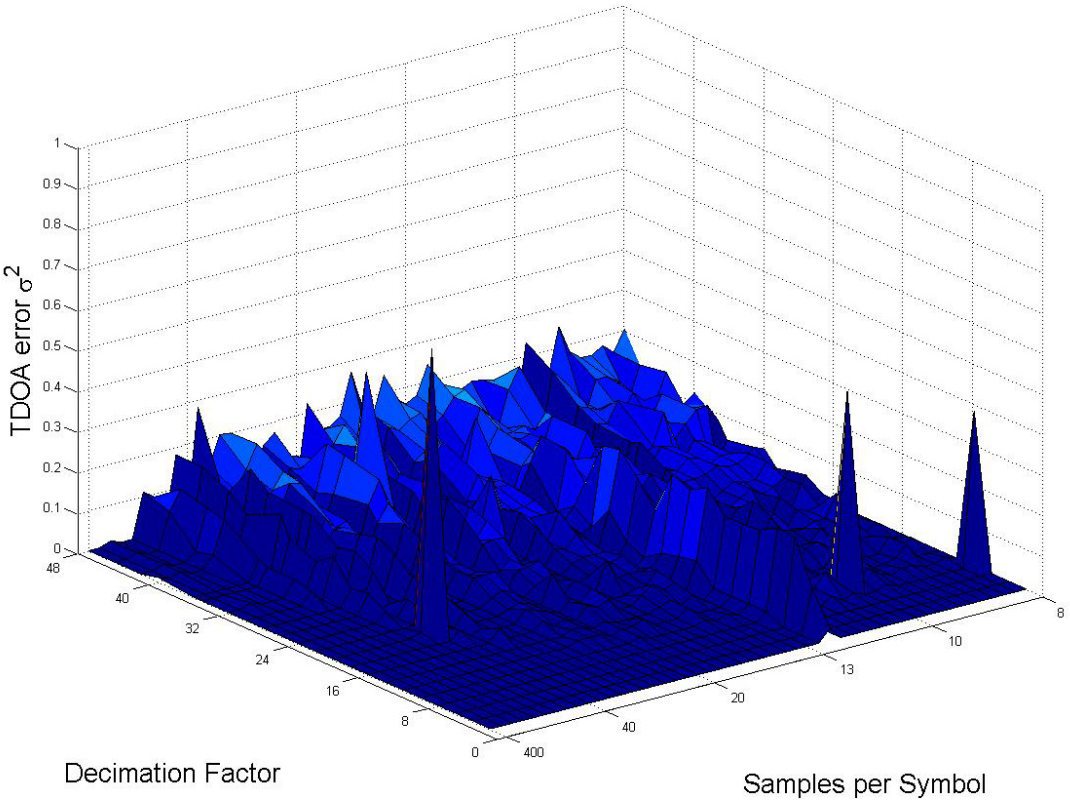

Figure 3.17 TDOA error as a function of symbol rate and decimation factor (raised-cosine, distributed)

Comparing the results of the decimation experiments for the rectangular pulse (Fig. 3.14) with those for the raised-cosine pulse (Fig. 3.16), it can be seen that for low decimation factors, the raised-cosine shaped signals produce less TDOA error than the rectangular shaped signals. However, for large decimation factors, the TDOA error for the rectangular shaped signals is slightly less than for the raised-cosine shaped signals. Figures 3.18a and 3.18b compare the TDOA error variance for both cases when the signals are decimated by the factors 10, 20, 30, and 42.

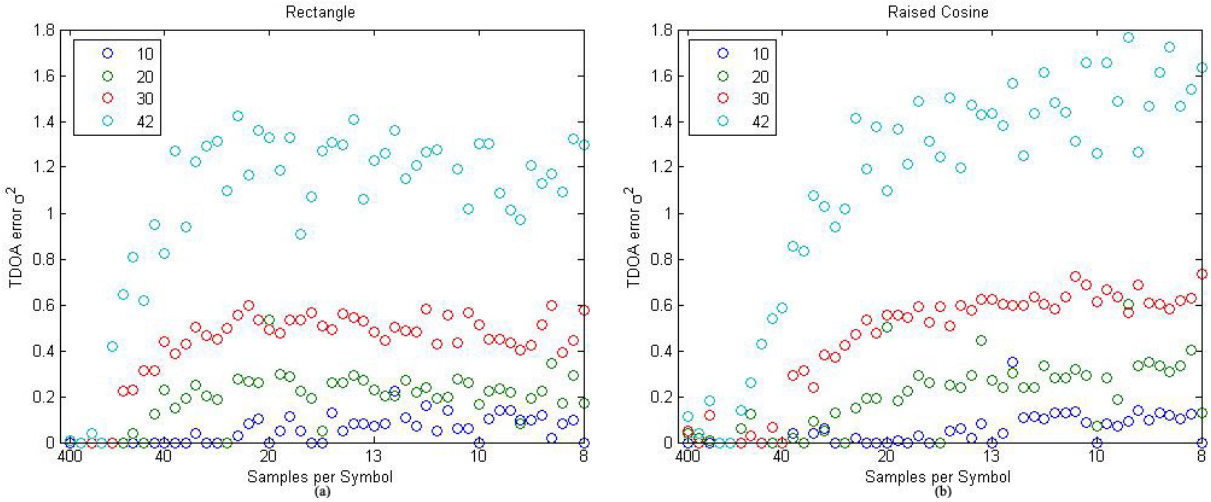

Figure 3.18 TDOA error as a function of symbol rate for decimation factors 10, 20, 30, 42

(a) rectangular shaped signal (b) raised-cosine shaped signal

The reason for this behavior may be explained by examining the spectral shape of the pulses. The PSD of the raised-cosine decays proportional to $1/f^6$; therefore, the power contributed by side lobes is less than the power contributed by the side lobes of the PSD of the rectangle (which decays proportional to $1/f^2$). Also, the central lobe of the PSD of the raised-cosine is wider than the central lobe of the PSD of the rectangle. Figure 3.19 depicts the amount power which is retained after decimating a rectangular pulse and a raised-cosine pulse.

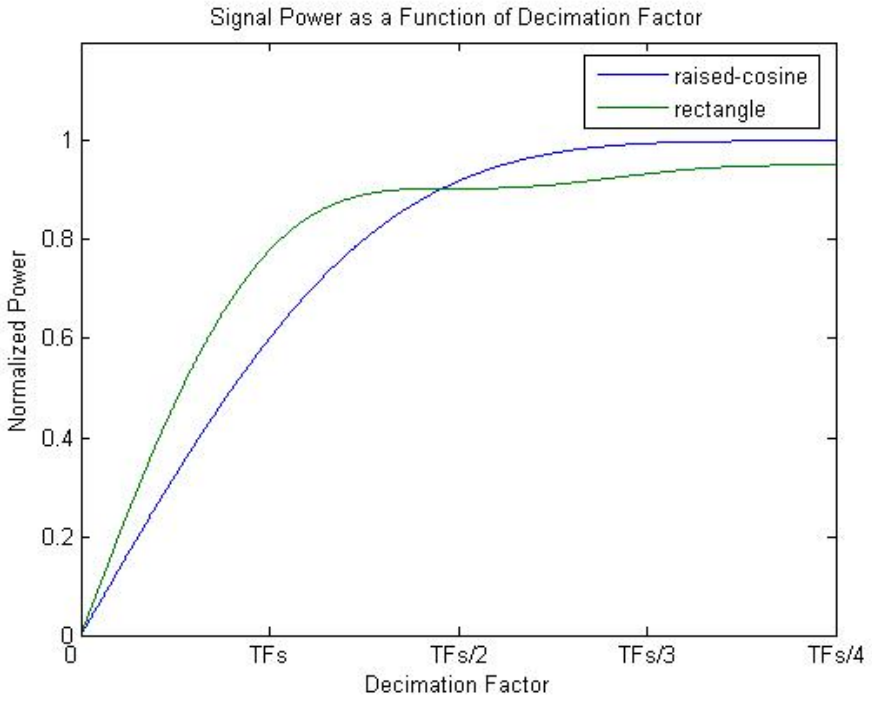

Figure 3.19 Signal power as a function of decimation factor
(Decimation removes energy from the signal)

When we decimate by small factors (but large enough to reduce the rate below the Nyquist rate), we are, in effect, removing side lobes from the signal; therefore, more energy will be removed from the signal shaped by a rectangular pulse. As a result, the signal-to-noise ratio of the interpolated rectangular pulse-shaped signal will be lower, which will, in turn, have a greater effect on the estimation error.

When we decimate by large factors (large enough to remove all side lobes), we remove power from the central lobe. The majority of the power in a raised-cosine pulse lies in its central lobe, in the region $|f| < \frac{2}{T}$, while the majority of the power in the rectangular pulse is in the central lobe, in the region $|f| < \frac{1}{T}$. Decimating the sampled, raised-cosine shaped signal by a factor, $L \geq \frac{TF_s}{4}$, will result in removing power from the central lobe; whereas, the central lobe of the rectangular shaped signal will not be affected until we decimate by a larger factor, $L \geq \frac{TF_s}{2}$. Notice (Fig. 3.19) that the rectangular shaped signal is decimated by factors greater than about

$\frac{TF_s}{2}$, it retains more power than the raised-cosine shaped signal, decimated by the same amount. This loss of power at higher decimation factors is what accounts for the improvement of the TDOA estimate for the rectangular shaped signal over the raised-cosine shaped signal.

Chapter 4

The Effects of Quantization

4.1 The Subband Encoder

In this chapter we will follow the work of [19-22] in developing a subband encoder which is designed to compress an intercepted signal while minimizing adverse effects on the TDOA estimation process. The observed signal is decomposed into a number of frequency subbands, each of which is quantized independently, using a uniform scalar quantizer. The structure of the subband codec is depicted in figure 4.1. The sequence that is being compressed, $x(n)$, is the sampled complex envelope of an observed signal, which is assumed to be finely quantized using 32 bits per sample. The real and imaginary parts of $x(n)$ are independently quantized; therefore, the compression ratio of the subband encoder can be calculated as $CR = {}^{32}\!/_{2R}$, where R is the number of bits budgeted per sample for the compressed signal.

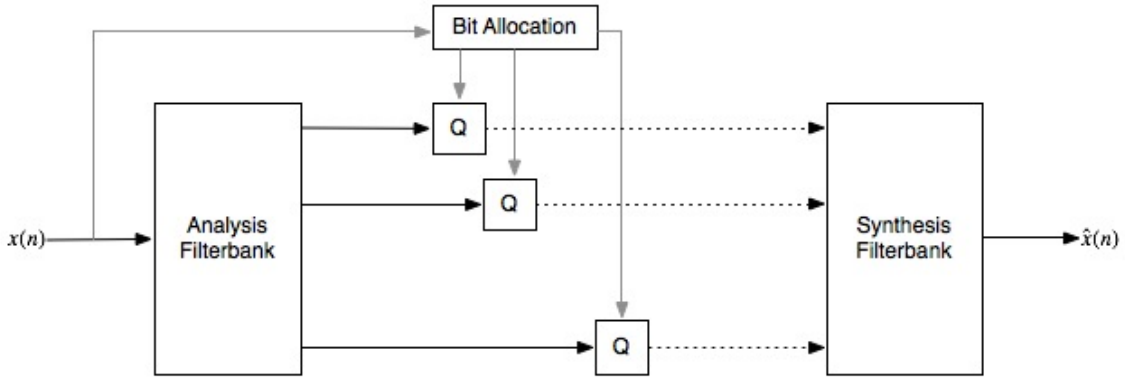

Figure 4.1 Subband encoder/decoder block diagram

The subband encoder consists of an M-channel Pseudo-QMF analysis filter bank (Section 2.6) and M uniform scalar quantizers. The bit allocation for the quantizers is determined by a fusion center which observes a portion of an intercepted signal. The focus of this chapter will be on comparing the effectiveness of a bit allocation determined using Fisher Information-based criteria versus choosing an allocation based solely on mean-squared-error distortion criteria.

4.2 Mean Squared Error Distortion Criteria

In order to establish a basis for comparison, we will first use the well-known MSE distortion criteria to determine a bit allocation for the subband encoder. We use the same rate-distortion model as in [19] for the i^{th} subband:

$$D_i(b_i) = {}^{\sqrt{3}\pi}\!/_{2}\, \sigma_i^2 2^{-2b_i}, 1 \le i \le M \qquad (4.1)$$

where the variance of the signal samples of the i^{th} subband, σ_i^2, is determined empirically from a portion of the signal. Using the M rate-distortion functions and a rate constraint, R, the bit allocation, B, is determined by solving the constrained integer optimization problem:

$$\min_{B}\left\{\sum_{i=1}^{M} D_i(b_i)\right\} \text{ subjec} \qquad \text{t to: } \left\{\sum_{i=1}^{M} b_i \le R\right\} \tag{4.2}$$

Where the bit allocation vector is $B = \{b_i \ge 0 | i \in 1,2,\cdots,M\}$.

To demonstrate the bit allocation process, we will use a rectangular pulse-shaped signal (Section 3.3) with a pulse duration, $T = 5ns$, sampled at the rate, $F_s = 20MHz$. Since the band-limited communication signal is oversampled, it can be downsampled prior to subband encoding without introducing significant error in the TDOA estimate (Chapter 3). The signal is downsampled by a factor of 16 so that the central lobe and two side-lobes of the power spectrum density are retained. The magnitude spectrum of the downsampled signal is shown in figure 4.2.

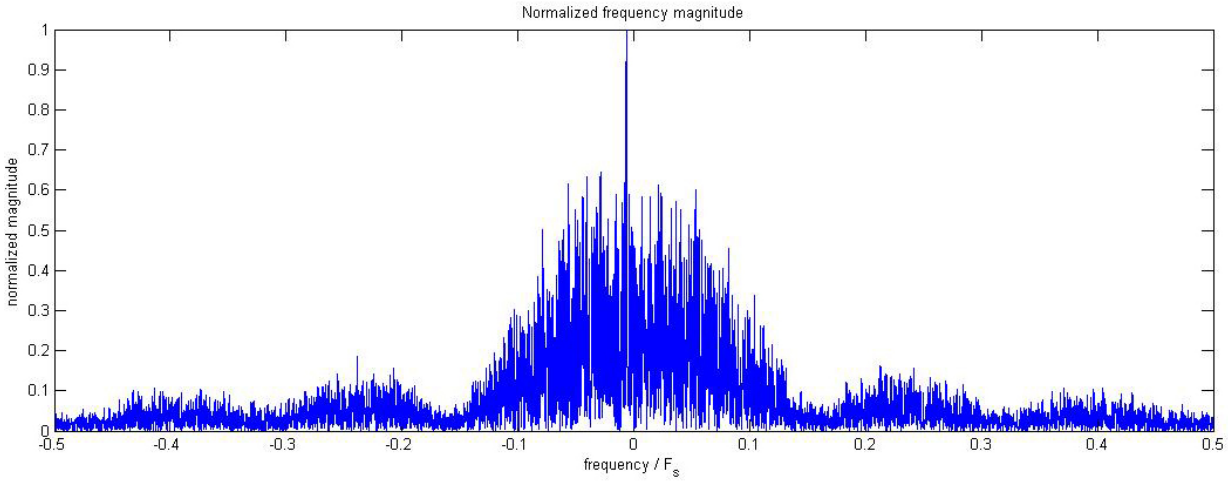

Figure 4.2 Magnitude spectrum of a rectangular shaped signal
(T=5ns, Fs=20MHz, SNR=10dB)

The signal is decomposed into 32 frequency subbands using a pseudo-QMF bank. Figure 4.3 depicts the variance of the subband samples, $\sigma_i^2, 1 \le i \le 32$.

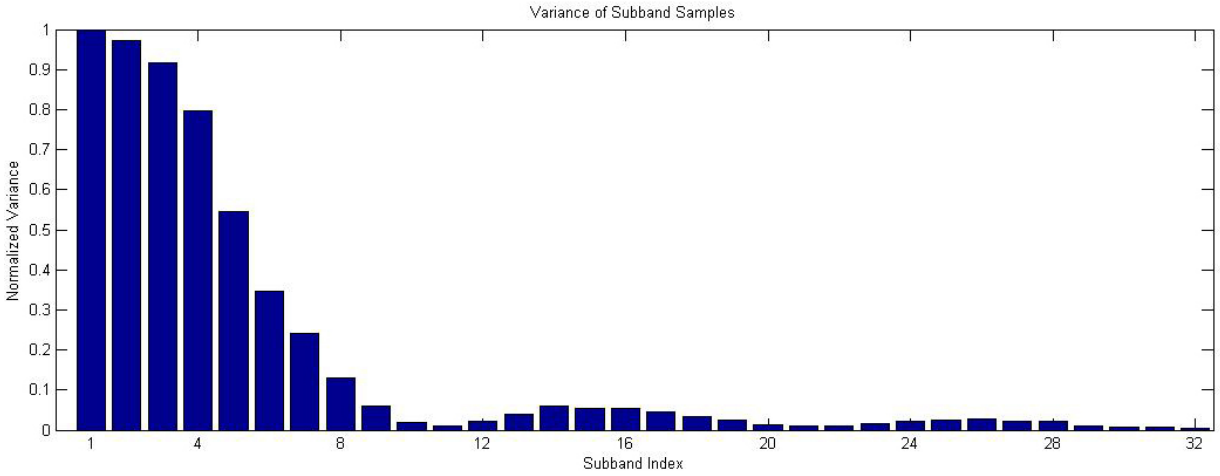

Figure 4.3 Variance of the subband samples

The variances, $\sigma_i^2, 1 \le i \le 32$, are then used in equation 4.1 to compute the rate-distortion functions for the 32 subbands. The rate-distortion functions, combined with the rate constraint, *R*, allow us to formulate the constrained optimization problem in equation 4.2. The optimization problem was solved using a MATLAB implementation of the Lagrange optimization algorithm described in Appendix A. Figure 4.4 depicts the 32 rate-distortion functions and the solution points, $b_i, 1 \le i \le M$, (red *x*'s) when the rate is constrained to 4 bits per sample (4:1 compression ratio).

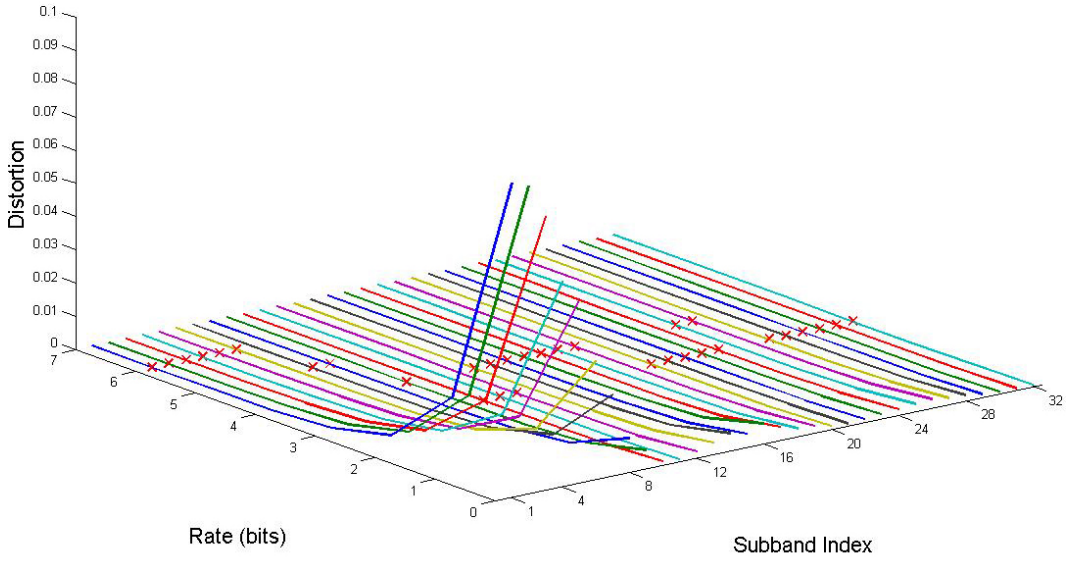

Figure 4.4 Rate-Distortion functions for the 32 quantizers (4:1 Compression Ratio)

The bit allocation, *B*, which provides a solution to the constrained optimization problem (Eq. 4.2), for this example is depicted in figure 4.5

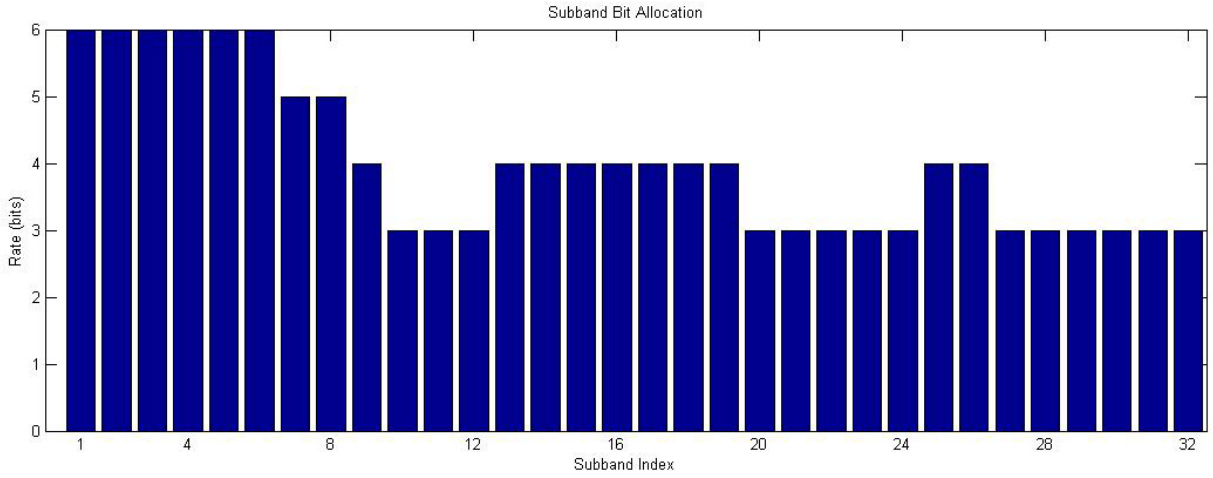

Figure 4.5 Bit allocation computed using MSE criteria

Notice that by using the MSE-based distortion criteria, bits are allocated to subbands based primarily on their power content. Since white noise was added to the signal prior to compression, the PSD of the noisy signal at high frequencies is nearly flat; therefore, the bits are allocated almost evenly over the side lobes.

4.3 Fisher Information Distortion Criteria

The Fisher Information-based distortion that we will use is that developed in [19-22] (Section 2.5). We will derive the Fisher Information (for TDOA) for the rectangular and raised cosine pulses (section 3.3) using the formulas introduced in section 2.6. Continuing with the power spectrum density of a rectangular pulse-shaped signal, sampled at the rate $1/T_s$ (Eq. 3.5):

$$\tilde{\phi}(f) = \frac{1}{T_s^2}\sigma_i^2 A^2 T\left(\frac{\sin \pi f T}{\pi f T}\right)^2, |f| \le F_s/2 \qquad (4.3)$$

Substituting the PSD of the signal into the Fisher Information formula that was presented earlier (Eq. 2.20), we have:

$$J = \frac{1}{\sigma_1^2 + \sigma_2^2}\int_{-F_s/2}^{F_s/2} f^2 \left\{\frac{1}{T_s^2}\sigma_i^2 A^2 T\left(\frac{\sin \pi f T}{\pi f T}\right)^2\right\} df \qquad (4.4)$$

The f^2 terms in the numerator and denominator of the integrand of equation 4.4 cancel and the Fisher Information becomes:

$$J = \frac{2\sigma_i^2 A^2}{(\sigma_1^2 + \sigma_2^2)\pi^2 T_s^2}\int_{-F_s/2}^{F_s/2} \sin^2 \pi f T df \qquad (4.5)$$

$$= \frac{2\sigma_i^2 A^2}{(\sigma_1^2 + \sigma_2^2)\pi^2 T_s^2} \int_{-F_s/2}^{F_s/2} (1 - \cos 2\pi f T) df \qquad (4.6)$$

As discussed in section 2.6, in the wireless sensor network scenario, it is assumed that we cannot observe the original signal, uncorrupted by additive noise. Additionally, it is assumed that the sensor which is performing the compression will know the variance of the noise at a neighboring sensor; therefore, it is not feasible to directly compute the Fisher Information (Eq. 4.6). Instead, we follow the approach of [19][22] and approximate the Fisher Information using the DFT coefficients of an intercepted, noisy signal (Eq. 2.25). To demonstrate the performance of the approximate FI model (Eq. 2.25), figure 4.6 compares the quadratically weighted DFT coefficients of an intercepted noisy signal to the integrand of equation 4.6 (where the integrand is sampled using the same number of points as the DFT).

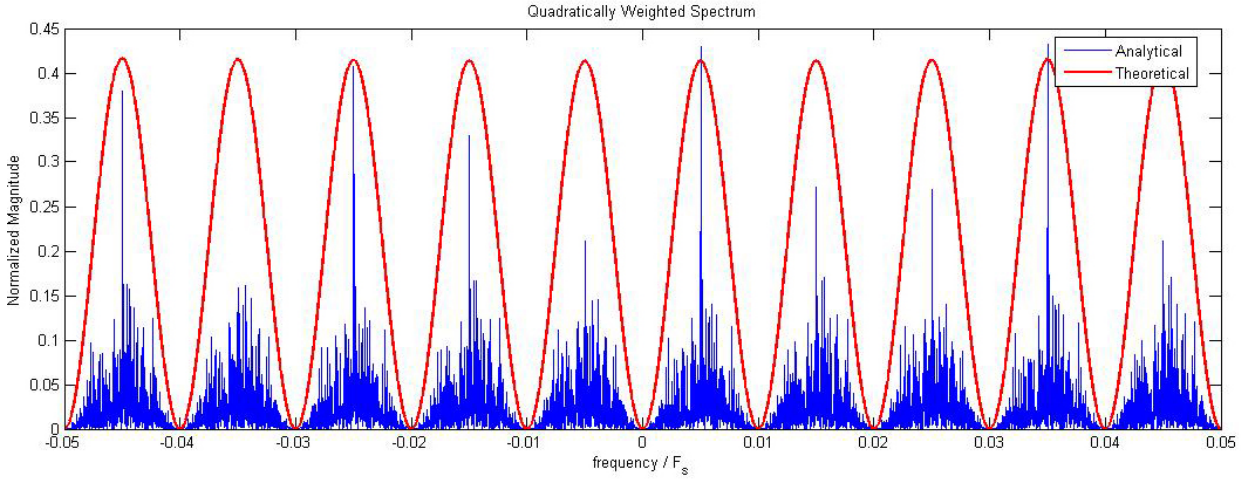

Figure 4.6 Quadratically weighted power spectrum of rectangular pulse shaped signal

Because the FI is proportional to the integral of the quadratically weighted PSD, we can examine the contribution of individual frequency components to the Fisher Information. Due to the form of the FI of the rectangular pulse-shaped signal (Eq. 4.6), it is apparent that the side lobes contribute significantly to the FI.

Similarly, for the raised-cosine pulse shaped signal (Eq. 3.6), it can be shown that the Fisher Information with respect to TDOA estimation is:

$$J = \frac{\sigma_i^2 A^2}{4(\sigma_1^2 + \sigma_2^2)\pi^2 T_s^2} \int_{-F_s/2}^{F_s/2} \frac{\sin^2 \pi f T}{(1 - f^2 T^2)^2} df \qquad (4.7)$$

Figure 4.7 depicts the integrand of equation 4.7 and the quadratically weighted DFT coefficients of an intercepted, noisy raised-cosine pulse-shaped signal. Notice that the weighted spectrum decays proportional to $1/f^4$, implying that frequency components in the range $|f| < \frac{2}{T}$ will contribute heavily to the Fisher Information.

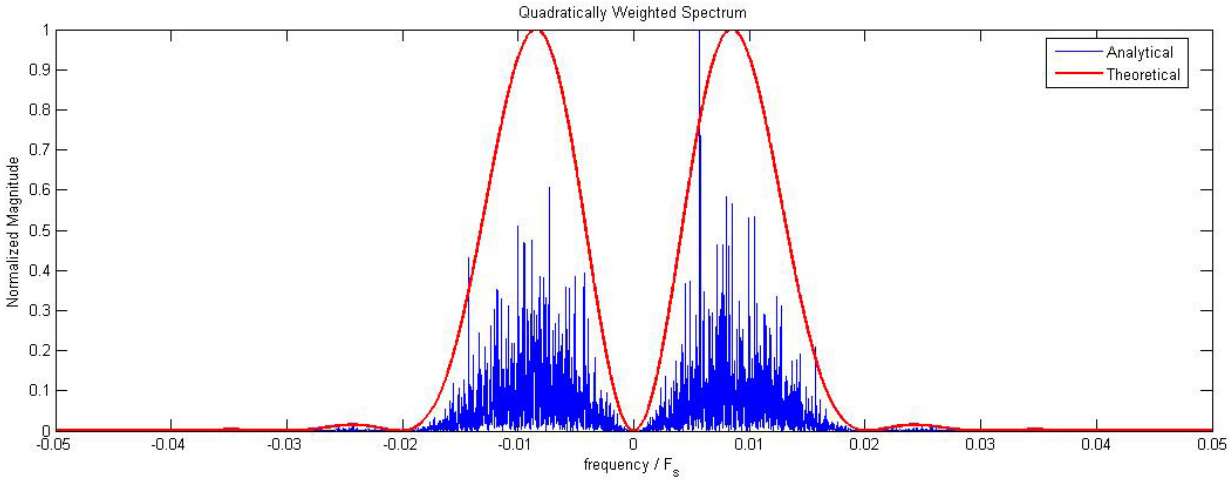

Figure 4.7 Quadratically weighted spectrum of raised-cosine

Following the work of [19-22], we use the Fisher Information-based model (Eq. 2.25, 2.26) to characterize the effects of quantization on the TDOA estimation process. The FI corresponding to the i^{th} subband for the multi-bit case is computed as [19][21]:

$$\tilde{J}_i^{(m)} = \frac{2\pi^2 \sum_{n \in N_i} n^2 \left|X[n]\right|^2}{N\sigma^2 + q_i^2} \qquad (4.8)$$

The distortion introduced by quantization of the i^{th} subband, q_i^2, is calculated using the rate-distortion model in equation 4.1. The FI corresponding to the i^{th} subband for the single-bit quantization case is computed as [19]:

$$\tilde{J}_i^{(1)} = \frac{4}{\pi N\sigma^2} \sum_{n \in N_i} n^2 \left| \mathrm{Im}^2\{X_i[n]\} \exp\left(-\frac{2}{N\sigma^2}\mathrm{Re}^2\{X_i[n]\}\right) \times \frac{1}{1 - erf^2(\mathrm{Re}\{X_i[n]\}/(\sqrt{N}\sigma))} \right| + \frac{4}{\pi N\sigma^2} \sum_{n \in N_i} n^2 \left| \mathrm{Re}^2\{X_i[n]\} \exp\left(-\frac{2}{N\sigma^2}\mathrm{Im}^2\{X_i[n]\}\right) \times \frac{1}{1 - erf^2(\mathrm{Im}\{X_i[n]\}/(\sqrt{N}\sigma))} \right| \qquad (4.9)$$

Where N_i is the set of indices belonging to the i^{th} subband. The bit allocation is then determined by solving the optimization problem:

$$\max_B \left\{ \sum_{i=1}^{M} \tilde{J}_i \right\} \qquad \text{subject to:} \qquad \left\{ \sum_{i=1}^{M} b_i \le R \right\} \qquad (4.10)$$

Where the bit allocation vector, $B = \{b_i \ge 0 | i \in 1,2,\cdots,M\}$, is constrained to non-negative integers and the objective function is:

$$\tilde{J}_i = \begin{Bmatrix} 0, b_i = 0 \\ \tilde{J}_i^{(1)}, b_i = 1 \\ \tilde{J}_i^{(m)}, b_i \geq 2 \end{Bmatrix} \tag{4.11}$$

A Lagrange optimization routine was implemented in MATLAB to solve the constrained minimization problem presented in section 4.2 (Eq. 4.2). If we could somehow reformulate the constrained maximization problem (Eq. 4.10) as a minimization problem, then we could use the same optimization procedure to solve for both the MSE-based and FI-based bit allocations. The objective function, $\tilde{J}_i$, is defined by 3 different functions (Eq. 4.11), depending on the value of the rate, b_i. Consider, first, the function, $\tilde{J}_i^{(m)}$, for multi-bit quantization (Eq. 4.8). Replacing the numerator of equation 4.8 by G, $\tilde{J}_i^{(m)}$ can be rewritten as:

$$\tilde{J}_i^{(m)} = \frac{G}{\sigma^2 + q_i^2} \tag{4.12a}$$

$$= \frac{G}{\sigma^2} - \frac{q_i^2 G}{\sigma^2(\sigma^2 + q_i^2)} \tag{4.12b}$$

$$= \frac{G}{\sigma^2} - \hat{J}_i^{(m)} \tag{4.12c}$$

Using equation 4.12b, the maximization problem (Eq. 4.10), for the case when $b_i \geq 2$ can be expressed as:

$$\max_B \left\{ \sum_{i=1}^{M} \tilde{J}_i^{(m)} \right\} = \max_B \left\{ \sum_{i=1}^{M} \left[\frac{G}{\sigma^2} - \frac{q_i^2 G}{\sigma^2(\sigma^2 + q_i^2)} \right] \right\} \tag{4.13}$$

Where $B = \{ b_i \geq 2 | i \in 1,2,\cdots,M \}$. Since q_i^2, by definition (Eq. 4.1), is the only term in equation 4.13 which is a function of b_i, the parameter over which we are searching, the optimization problem (Eq. 4.13) can be equivalently stated as [22]:

$$\min_B \left\{ \sum_{i=1}^{M} \left[\frac{q_i^2 G}{\sigma^2(\sigma^2 + q_i^2)} \right] \right\} = \min_B \left\{ \sum_{i=1}^{M} \hat{J}_i^{(m)} \right\} \tag{4.14}$$

Where $B = \{ b_i \geq 2 | i \in 1,2,\cdots,M \}$. Similarly, we reformulate the values of the objective function of the maximization problem (Eq. 4.11) for the single-bit ($b_i = 1$) and zero-bit ($b_i = 0$) cases:

$$\hat{J}_i^{(1)} = \frac{G}{\sigma^2} - \tilde{J}_i^{(1)} \tag{4.15}$$

$$\hat{J}_i^{(0)} = \frac{G}{\sigma^2} \tag{4.16}$$

The bit allocation can now be determined by solving the optimization problem:

$$\min_{B}\left\{\sum_{i=1}^{M}\hat{J}_i\right\} \qquad \text{subject to:} \qquad \left\{\sum_{i=1}^{M}b_i \le R\right\} \tag{4.17}$$

Where $B=\{b_i \ge 0 | i \in 1,2,\cdots,M\}$ and the objective function is defined as:

$$\hat{J}_i=\begin{Bmatrix}\frac{G}{\sigma^2},b_i=0\\ \hat{J}_i^{(1)},b_i=1\\ \hat{J}_i^{(m)},b_i\ge 2\end{Bmatrix} \tag{4.18}$$

Figure 4.8 depicts the objective functions (Eq. 4.17) computed for a 32 subband encoder. The red *x*'s denote the solution points, $b_i, 1 \le i \le M$, to the optimization problem when the rate was constrained to 4 bits per sample (4:1 compression ratio).

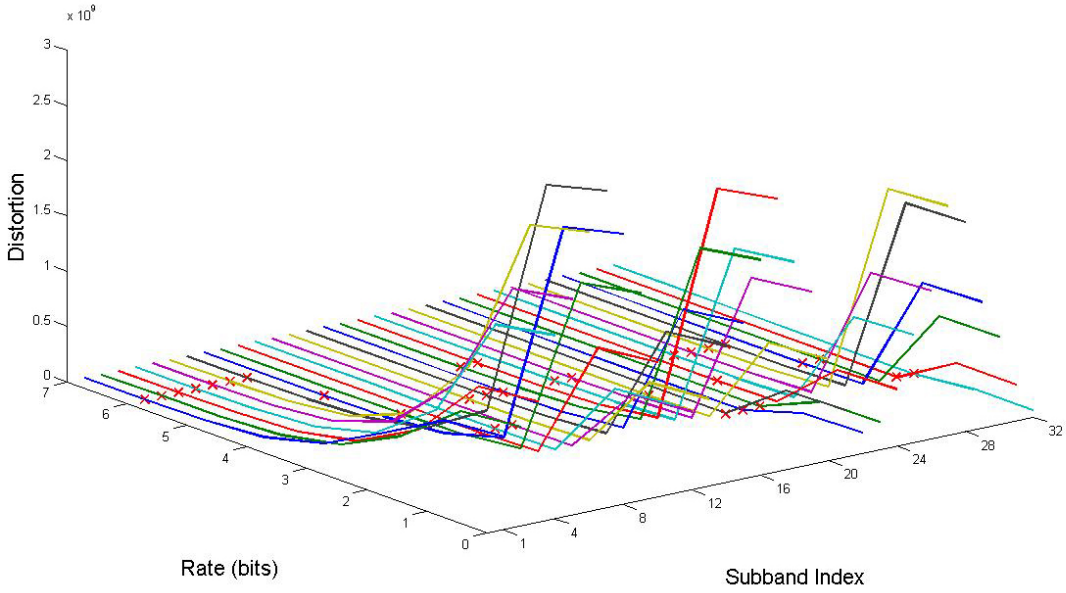

Figure 4.8 FI-based objective function for the 32 quantizers (4:1 Compression Ratio)

Notice that the objective functions in figure 4.8 are not convex due to the values given by the single-bit approximation. As a result of the non-convexity, the Lagrange optimization algorithm (section 2.4) used to solve the constrained optimization problem (Eq. 4.17) may not yield an optimal solution. Instead, we use the Lagrange optimization procedure to find the closest solution from below (a rate which is less than or equal to the constraint), then we use a water-filling method (Appendix A) to allocate any remaining bits. Figure 4.9 depicts the bit allocation determined by solving the constrained optimization problem (Eq. 4.17).

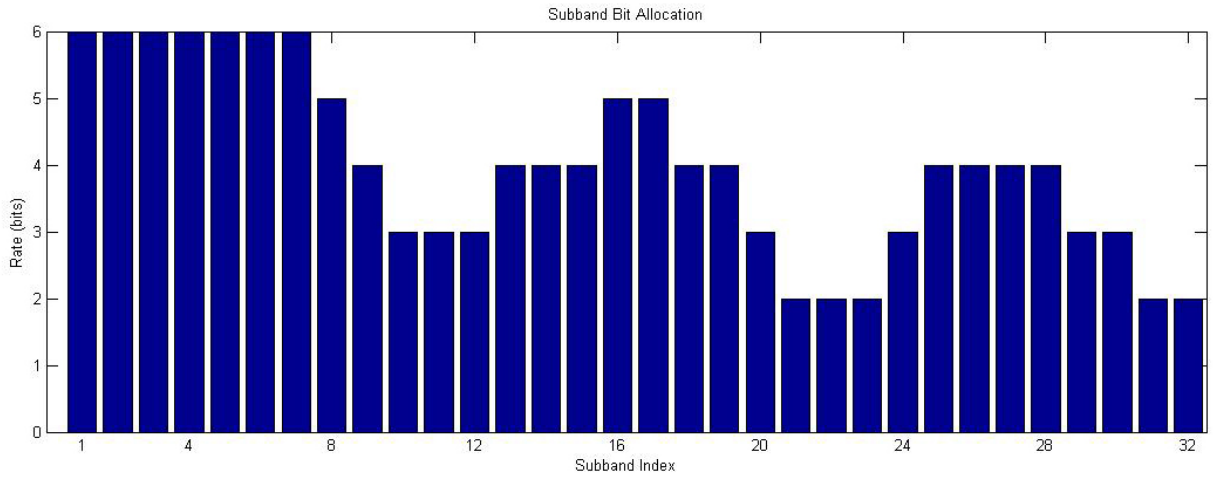

Figure 4.9 Bit allocation computed using FI-based criteria

Notice that more bits are allocated to the side lobes when we use the FI-based approach (due to quadratic weighting of the spectrum). In the MSE-based approach, the bits were allocated more evenly in the subbands which contain the side lobes.

4.4 Experimental Results

We conducted a series of subband encoding experiments to compare the performance of using a bit allocation determined via MSE-based criteria versus a bit allocation determined by the FI-based approach. In the experiments, linearly modulated signals were randomly generated and had an average duration of 3 ms (60,000 samples with $F_s = 20MHz$). The signals were decimated prior to subband encoding to enhance the TDOA error introduced by fine quantization (as a coarsely quantized signal can still provide an error-free TDOA estimate when the number of samples is very large). Figure 4.10 depicts the codec that was used in the experiments.

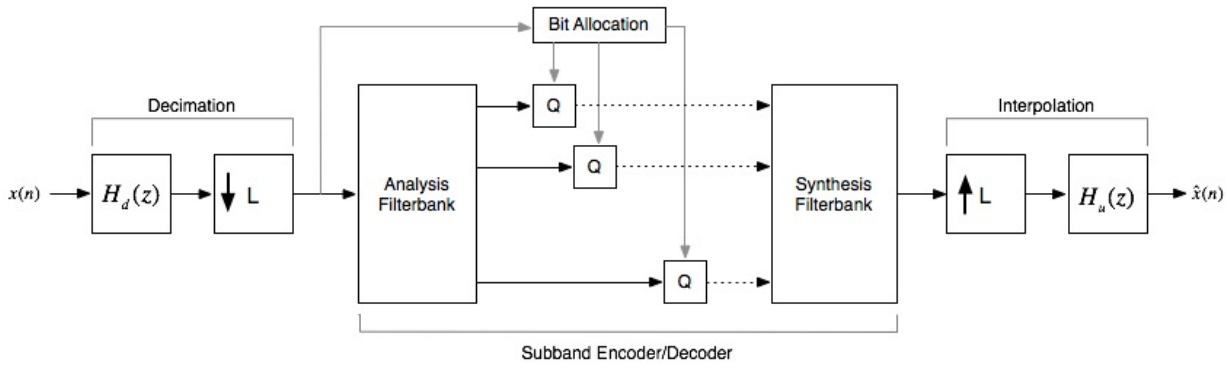

Figure 4.10 Codec block diagram

We selected the symbol rates and decimation factors using data obtained from the decimation experiments (Chapter 3). Figure 4.11 depicts 3 operating points that were chosen for the experiments with a rectangular pulse-shaped signal.

Table 4.1 Operating points for subband encoding experiments

Operating Point	Symbol Rate (samples/symbol)	Decimation Factor
1 100		48
2 19		14
3 9		8

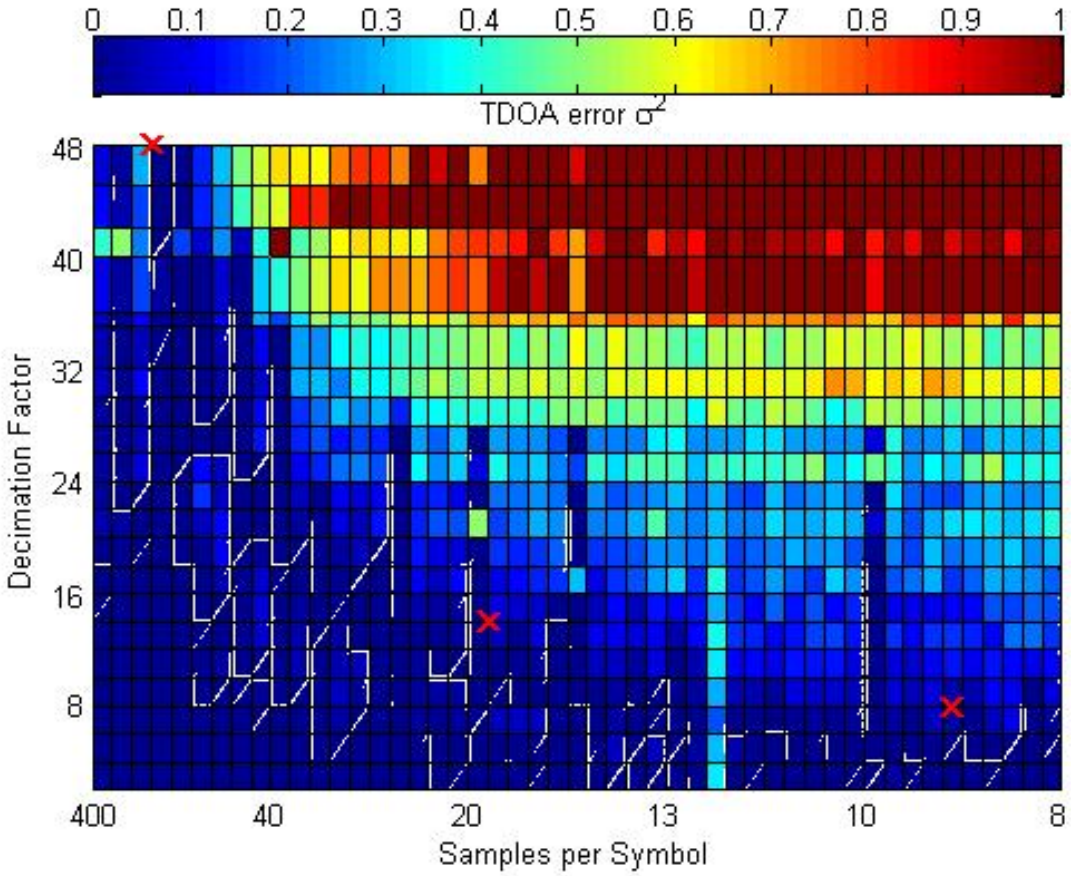

Figure 4.11 Operating points for subband encoding experiments
(rectangular pulse-shaped signal)

The red regions in figure 4.11 indicate large TDOA error whereas the dark blue regions indicate very small TDOA estimation error. The operating points were chosen to be in regions where decimation produced little to no error, but where further decimation would result in a sizeable increase in error.

In the first set of experiments, we randomly generated 100 signals and independently computed a bit allocation for each received signal. A fixed compression ratio was chosen and the SNR of two signals (received by two different sensors) was varied from 40dB to 10dB. The scenario of centralized estimation (where two sensors compress their observed signals prior to transmitting

them to a fusion center for processing) was simulated. The compressed/decompressed signals were used to obtain a TDOA estimate, which was then compared to a TDOA estimate obtained from signals which had not been compressed (then decompressed).

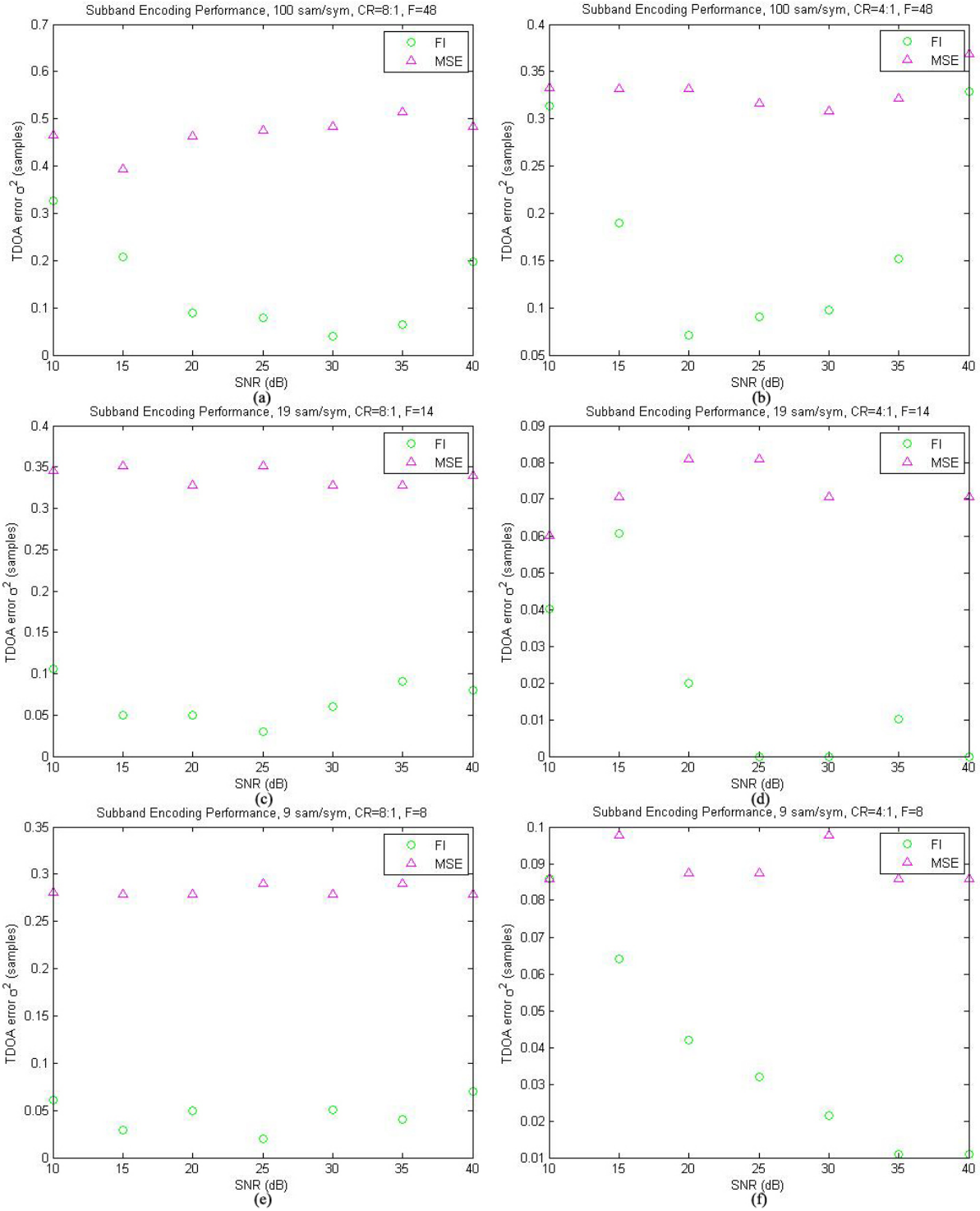

Figure 4.12 Subband encoder performance using bit allocation for each signal (a) exp 1, CR=8:1 (b) exp 1, CR=4:1 (c) exp 2, CR=8:1 (d) exp 2, CR=4:1 (e) exp 3, CR=8:1 (f) exp 3, CR=4:1

Figures 4.12 and 4.14 depict the results of the experiment performed at the 3 different operating points (table 4.1). Figures 4.12 (a) and (b) (top) present the results for operating point 1, figures 4.12 (c) and (d) (middle) present the results for operating point 2, and figures 4.12 (e) and (f) (bottom) present the results for operating point 3. Figures 4.12 (a),(c), and (e) (left) depict the results when the compression ratio was fixed at 8:1, and Figures 4.12 (b),(d), and (f) (right) depict the results when the compression ratio was fixed at 4:1.

Notice (Fig. 4.12) that subband encoding using the FI-based approach resulted in less TDOA estimation error than the MSE-based approach. According to the approximate FI model that was used for compression (Eq. 4.8, 4.9), the FI should increase as the signal-to-noise ratio of the received signal is increased, meaning that the TDOA error variance should decrease. Observing the experimental results (Fig. 4.12), it is apparent that, in general, the TDOA estimation error is decreasing as the SNR is increased up to about 25dB. In most cases (Fig. 4.12(a-e)), the estimation error increases as the SNR is increased above 25dB. Referring back to the approximate FI model (Eq. 4.8, 4.9), we mentioned that a necessary condition for the model to hold was that the variance of the noise introduced by quantization remains smaller than the variance of the sensor noise. When the signal-to-noise ratio becomes large, the variance of the sensor noise becomes small and the approximate FI model fails to hold.

The approach of calculating a bit allocation for each received signal can be computationally expensive for wireless sensors and also requires additional side information to be included with each compressed signal. We subsequently explored a suboptimal approach which would not require computation of a bit allocation for each received signal. In the second set of experiments, 100 signals were generated at random, as before, but only one of the signals was analyzed to determine the bit allocation which would be used to compress all 100 signals. To demonstrate the selection of a bit allocation, figure 4.13(a) compares the average of the allocations calculated for 100 randomly generated signals, using FI criteria, to the allocations calculated for two randomly selected message signals 4.13(b) and (c).

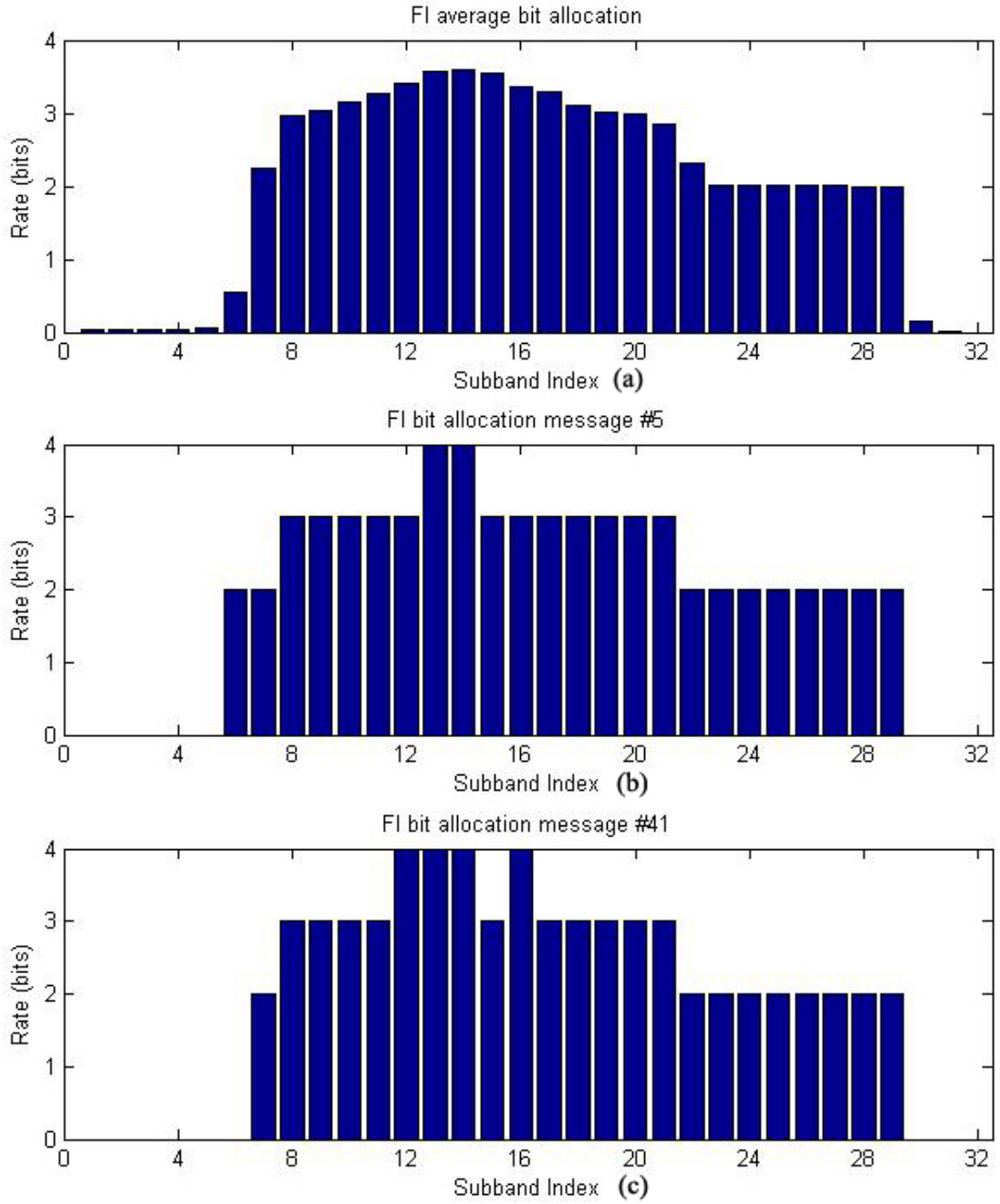

Figure 4.13 FI-based bit allocation (a) averaged over 100 messages
(b) message #5 (c) message #41

Figure 4.14 depicts the results of the experiment using the suboptimal approach, performed at the 3 operating points (table 4.1).

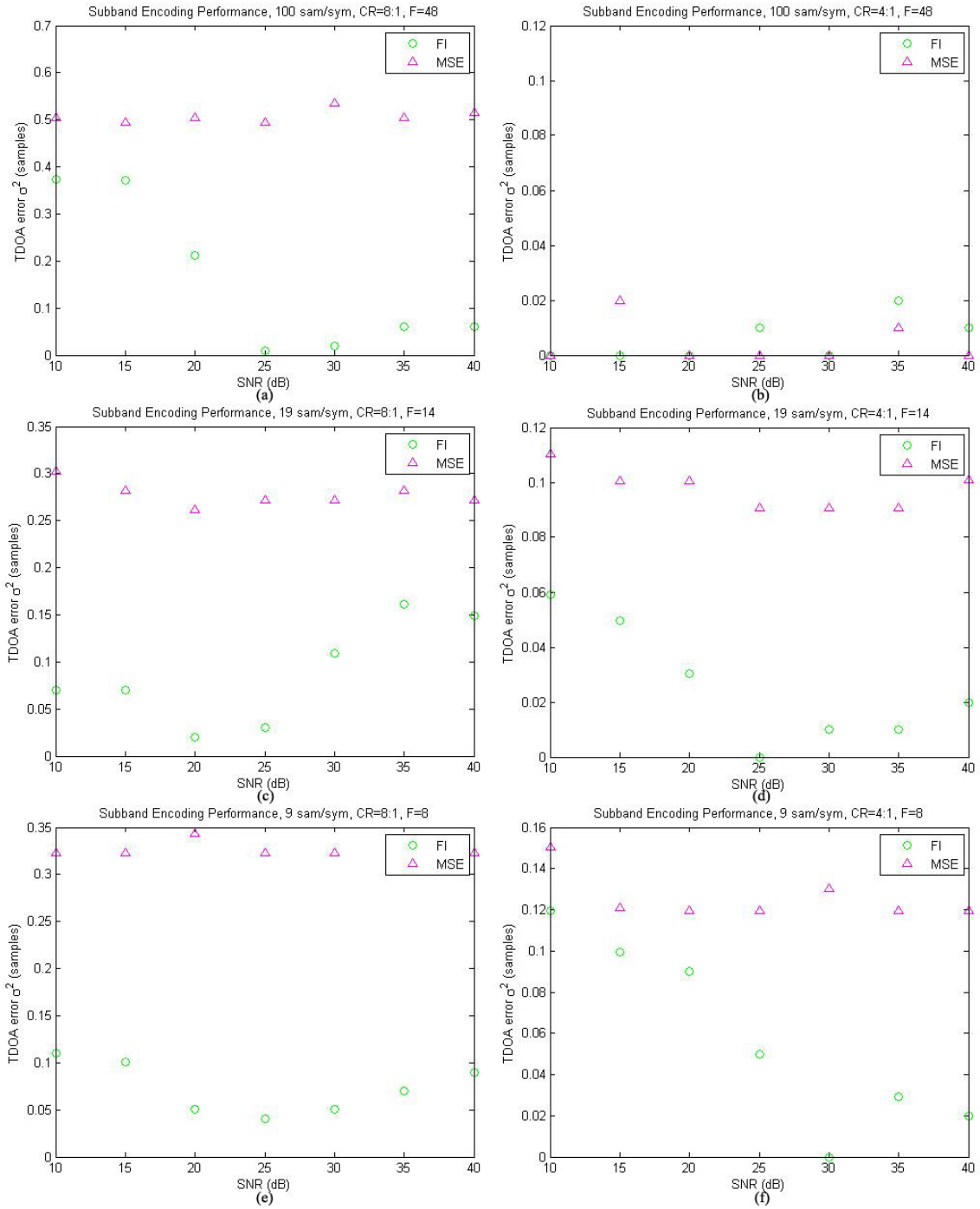

Figure 4.14 Subband encoder performance using one-time bit allocation
(a) exp 1, CR=8:1 (b) exp 1, CR=4:1 (c) exp 2, CR=8:1 (d) exp 2, CR=4:1
(e) exp 3, CR=8:1 (f) exp 3, CR=4:1

Figures 4.14 (a) and (b) (top) present the results for operating point 1, figures 4.14 (c) and (d) (middle) present the results for operating point 2, and figures 4.14 (e) and (f) (bottom) present the results for operating point 3. Figures 4.14 (a),(c), and (e) (left) depict the results when the

compression ratio was fixed at 8:1, and Figures 4.14 (b),(d), and (f) (right) depict the results when the compression ratio was fixed at 4:1.

It can be seen (Fig. 4.14) that, in general, the FI-based approach results in less TDOA estimation error than the MSE-based approach. In most cases, the error decreases as the SNR is increased until about 25dB. As the SNR is increased above 25dB, the error, in some cases, increases (similar to the first set of experiments). Notice in figure 4.14(b) that the error seems to fluctuate as the SNR in increased. This behavior is likely a results of using the suboptimal approach; however, also note that the error is nearly zero.

In comparing the results from the first set of experiments (Fig. 4.12) to the results of using the suboptimal approach (Fig. 4.14), it can be seen that in some cases (b, c, and d) that the suboptimal approach actually produced less error. For the other cases (a, e, f), the increase in error resulting from the suboptimal approach was reasonably small.

Upon observing the results of the experiments which were performed, (Fig. 4.12, 4.14), one can conclude that the approximate FI model (Eq. 4.8, 4.9) characterized the effects of quantization on the estimation task reasonably well. Additionally, the suboptimal approach of using a fixed bit allocation to compress an ensemble of messages produced good results.

Chapter 5

Conclusion

5.1 Discussion

In this thesis, we explored the effects of compression on the task of estimating time-difference-of-arrival parameters. We began by investigating, experimentally, the effects of decimation on TDOA estimation for digital linearly modulated signals with different symbol rates, using both rectangular and raised-cosine pulse-shaping transmit filters. We showed that the band-limited communication signals that were used could be decimated without introducing considerable error, so long as the power within the central lobe of the power spectrum was retained.

We next explored the effects of quantization on the estimation task using a Fisher Information-based model developed in [18-22]. Due to the structure of the FI model (Eq. 4.8) we implemented a subband encoder which would allow us to selectively quantize frequency subbands based on their contribution to the Fisher Information. We, additionally, developed a suboptimal algorithm to perform subband encoding by analyzing only a portion of the signals that were to be compressed. Experimental results showed that subband encoding using the FI-based approach resulted in less TDOA estimation error than using the standard MSE-based distortion criteria.

5.2 Further work

In order to characterize the effects of quantization on the TDOA estimation process, we used a Fisher Information-based model (Eq. 4.8, 4.9) developed in [18-22]. The model relies on the assumptions that 1) the sensor noise is i.i.d. AWGN, 2) the noise introduced by quantization is uniformly distributed, white, and independent of the sensor noise [19], and 3) the variance of the sensor noise is much larger than the variance of the quantization noise. When the intercepted signal is coarsely quantized or its SNR is high, conditions 2 and 3 will be violated and the FI model (Eq. 4.8) will not hold [22]. In [19], the authors provide an approximate model for the case of single-bit quantization (Eq. 4.9). Under high SNR conditions, the author of [22] provides a method for approximating the Fisher Information which is of large complexity, and is likely not feasible for use in resource constrained, real-time tracking scenarios. There remains further research in developing a FI model of low complexity which can hold under high SNR conditions.

Similar to the FI-based model developed for quantization [18-22], one could explore models to characterize the effects of decimation and subsequent interpolation on the TDOA estimation process.

Another possible avenue of research would be to compare the performance of decimation to the performance of quantization for compressing signals for TDOA estimation. In addition to analyzing the effects on the estimation task, one could include an analysis of the computational complexity of both methods.

Continuing under the framework of subband encoding for TDOA estimation, one could perform further analysis to determine the importance of different frequency subbands to the estimation task. In this thesis, we used an FI-based model which essentially applied a quadratic weighting to the spectrum of the signal which was to be compressed. Perhaps, with further analysis, one could determine the role which different frequency components play on the estimation of the TDOA parameter.

Bibliography

[1] A.H. Sayed, A. Tarighat, N. Khajehnouri, Network-based wireless location," *IEEE Signal Processing Magazine*, vol. 22, pp. 24-40, July 2005.

[2] Alcatel-Lucent, "Lucent Technologies and Clearnet conduct market trial of location-specific, personal mobile Internet services," November 2000, [Online Reference] Available, HTTP: http://www1.alcatel-lucent.com/gsearch/accessFile.jhtml?sendURL=http%3A//www.alcatel-lucent.com/wps/DocumentStreamerServlet%3FLMSG_CABINET%3DDocs_and_Resource_Ctr%26LMSG_CONTENT_FILE%3DInfo_and_Policies/infodev_alcatel_en.pdf&sendCollection=root&sendTitle=Report+by+Alcatel+and+Infodev%3A+promoting+private+sector+investment+and+innovation&specialColl=

[3] D. J. Torrieri, "Statistical theory of passive location systems," *IEEE Transactions on Aerospace and Electronic Systems*, vol. AES-20, no. 2, pp. 183-198, March 1984.

[4] S. Stein, "Differential delay/Doppler ML estimation with unknown signals," *IEEE Trans. Signal Processing*, vol. 41, pp. 2717-2719, August 1993.

[5] J. Aravena, G. Gu, J. Luo, "Enhanced TDOA/FDOA-Based Geolocation Algorithms"

[6] A. Ortega, K. Ramchandran, "Rate distortion methods for image and video compression," *IEEE Signal Processing Magazine*, vol. 15, pp. 23-50, November 1998

[7] G. Strang, T. Nguyen, *Wavelets and Filter Banks*, Wellesley-Cambridge Press, 1996

[8] J. H. Rothweiler, "Polyphase Quadrature Filters - a New Subband Coding Technique," *Proc. of the Int. Conf. IEEE ASSP*, vol. 8, pp. 1280-1283, Boston 1983.

[9] J. Proakis, M. Salehi, *Communication Systems Engineering*, NJ: Prentice Hall, 2002.

[10] J. Proakis, *Digital Communications*, McGraw-Hill, 2001.

[11] R. Gray, D. Neuhoff, "Quantization," *IEEE Transactions Information Theory*, vol. 44, pp. 1-63, October 1998.

[12] M. Cover, J. Thomas, *Elements of Information Theory*, Wiley Series in Telecommunications, 1991.

[13] S. Lloyd, "Least Square Quantization," *IEEE Transactions on Information Theory*, vol. 28, no. 2, pp. 129-137, 1982.

[14] Y. Shoham, A. Gersho, "Efficient bit allocation for an arbitrary set of quantizers," *IEEE Transactions on Acoustics, Speech, and Signal Processing*, vol. 36, pp. 1445-1453, September 1988.

[15] S. Stein, "Algorithms for Ambiguity Function Processing," *Transactions on Acoustics, Speech, and Signal Processing*, vol. 29, pp. 588-599, June 1981.

[16] B. Friedlander, "On the Cramer-Rao Bound for Time Delay and Doppler Estimation," *IEEE Transactions on Information Theory*, vol. IT -30, No. 3,pp. 575-580, May 1984.

[17] S. Kay, *Fundamentals of Statistical Signal Processing: Estimation Theory*, Englewood Cliffs, NJ: Prentice Hall, 1993.

[18] M.L. Fowler, M. Chen, "Optimizing Non-MSE Distortion for Data Compression in Emitter Location Systems," Conference on Information Sciences and Systems, Johns Hopkins University, March 12-14, 2003.

[19] M.L. Fowler, M. Chen, "Fisher-Information-Based Data Compression for Estimation Using Two Sensors," *IEEE Transactions on Aerospace and Electronic Systems*, July 2005, pp. 1131-1137.

[20] M.L. Fowler, M. Chen, "Geometry-Adaptive Data Compression for TDOA/FDOA Location," IEEE ICASSP 2005, Philadelphia, PA, March 18-23, 2005, vol. 4, pp. 1069-1072.

[21] M.L. Fowler, M. Chen, "Evaluating Fisher Information From Data for Task-Driven Data Compression," *IEEE 40th Annual Conference on Information Sciences and Systems*, pp. 967-972, March 2006.

[22] M. Chen, "Data Compression for Inference Tasks in Wireless Sensor Networks," PhD Dissertation, Binghamton University SUNY, 2006

[23] T. Nguyen, "Near-Perfect-Reconstruction Pseudo-QMF Banks," *IEEE Transactions on Signal Processing*, vol. 42, pp. 65-72, January 1994.

[24] T. Nguyen, "Digital filter bank quadratic-constrained formulation," *IEEE Transactions on Signal Processing*, vol. 43, pp. 2103-2108, September 1995.

[25] *Coding of Moving Pictures and Associated Audio for Digital Storage Media at up to about 1.5 MBIT/s*, ISO/IEC 11172-3

[26] J. Proakis, D. Manolakis, *Digital Signal Processing: Principles, Algorithms, and Applications*, Pearson, 1996.

[27] H. Everett, "Generalized Lagrange multiplier method for solving problems of optimal allocation of resources," *Operations Research*, vol. 11, pp. 399-417, 1963

[28] C. Shannon, "A Mathematical Theory of Communication," 1948

Appendix A: Lagrange optimization algorithm

Given a set of discrete (monotonically decreasing) rate-distortion functions, $D_i(R), 1 \le i \le M$, and a rate constraint *R*, the Lagrange optimization algorithm will determine an optimal way to distribute a budgeted set of bits to a set of quantizers . The optimization problem which we are trying to solve is:

$$\min_B \left\{ \sum_{i=1}^{M} D_i(b_i) \right\} \text{ subjec} \qquad \text{t to: } \sum_{i=1}^{M} b_i \le R \qquad \text{(A.1)}$$

where $B = \{ b_i \ge 0 | i \in 1,2,\cdots,M \}$. The set of admissible bit allocation values, b_i, is constrained to non-negative integers.

Introducing a Lagrange multiplier, $\lambda \ge 0$, references [4][16] show that the solution to the unconstrained problem:

$$\min_B \left\{ \sum_{i=1}^{M} D_i(b_i) + \lambda b_i \right\} \qquad \text{(A.2)}$$

is also the solution to the budget-constrained problem in equation A.1Moreover, they show that for a given λ:

$$\min_B \left\{ \sum_{i=1}^{M} D_i(b_i) + \lambda b_i \right\} = \sum_{i=1}^{M} \min_{b_i} \{ D_i(b_i) + \lambda b_i \} \qquad \text{(A.3)}$$

As a result, the minimum of the "Lagrangian cost function", $D_i(b_i) + \lambda b_i$, can be computed independently for each quantizer. Figure A.1 presents a graphical interpretation of minimizing the Lagrangian cost function.

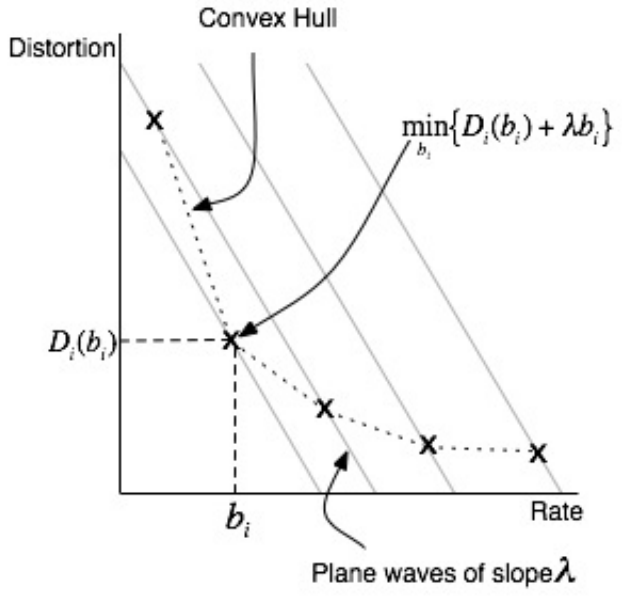

Figure A.1 Graphical interpretation of minimizing the Lagrangian cost function

As the rate, b_i, increases, the distortion, $D_i(b_i)$, decreases; therefore, we have a trade-off between rate and distortion. The Lagrange multiplier allows us to select specific trade-off points. Minimizing the Lagrangian cost function when $\lambda = 0$ is equivalent to minimizing the distortion; and minimizing the Lagrangian cost when $\lambda \to \infty$ is equivalent to minimizing the rate. As can be seen in figure A.1, the point in the rate-distortion function of the i^{th} quantizer which minimizes the Langrangian cost is that point at which the line of absolute slope λ is tangent to the convex hull of the rate-distortion function.

The optimization algorithm iteratively searches for a Lagrange multiplier, λ, which yields a solution that meets the predetermined rate constraint. The choice of an initial Lagrange multiplier, λ_i, will greatly affect the rate of convergence; therefore, λ_i was chosen as a function of the rate constraint, *R*. We used the algorithm discussed in [16] to search for a value, λ, which meets the rate constraint. Figure A.2 is a flow diagram of the algorithm which was implemented (using the notation from [16]). When an exact solution cannot be found using the Lagrange optimization alone, the Lagrange optimization is used to find the closest solution from below, then a water-filling method is used to allocate any remaining bits (Approximate Solution at bottom-right of Fig. A.2).

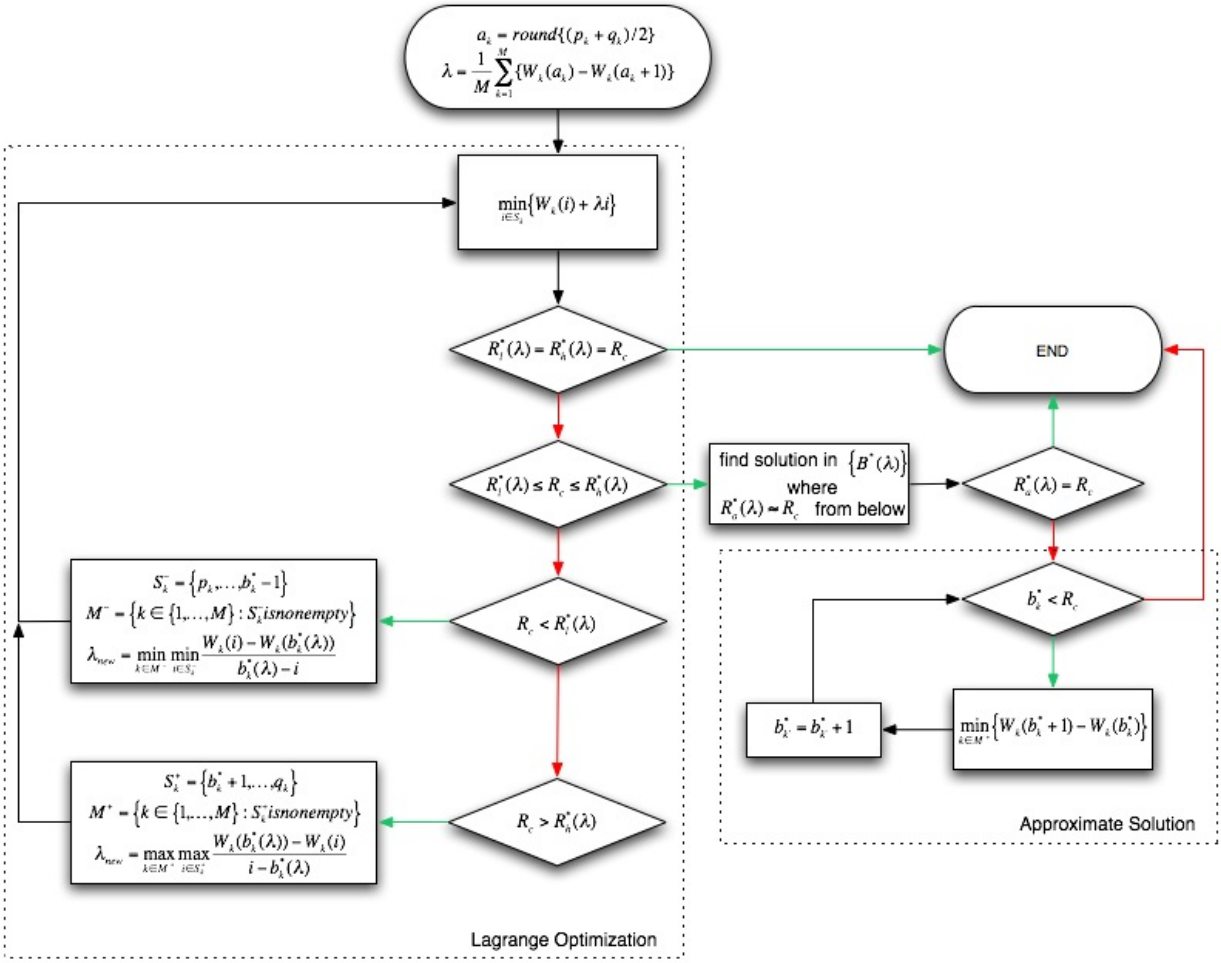

Figure A.2 Flowchart of Lagrange optimization algorithm (with water-filling)

The Lagrange multiplier-based optimization algorithm will provide an optimal solution so long as the discrete rate-distortion functions are convex and contain points which provide a solution for a given rate constraint (i.e. if the set of admissible bit allocation values, b_i, is further constrained, an optimal solution may be unreachable).

Appendix B: Additional Formulations

B.1 Cramer-Rao bound for time delay estimation

This appendix gives an outline of the derivation of the Cramer-Rao bound for time delay estimation. For a detailed formulation, the reader is directed to the sources from which the outline was created [4][15][16][17].

The Cramer-Rao inequality expresses an asymptotic lower bound on the variance of an unbiased statistical estimator. The reciprocal of the Fisher Information, $J(x;\theta)$, of the parameter θ, is the lower bound on the variance of an unbiased estimator of the parameter $\hat{\theta}$.

$$\mathrm{cov}\{\hat{\theta}\} \geq J^{-1} \tag{B.1}$$

Consider the problem of estimating a parameter vector θ from sample values of an *n*-variate time series $x(t)$. The elements of the Fisher Information for an unbiased estimator $\hat{\theta}$ are given by:

$$J_{ij}(x;\theta) = -E\left\{\frac{\partial^2 \ln p(x;\theta)}{\partial\theta_i \partial\theta_j}\right\} \tag{B.2}$$

Where $p(x;\theta)$ is the conditional probability density function. For the case where the elements of x are jointly Gaussian, Bangs has shown that the elements of the Fisher Information matrix are given by:

$$J_{ij} = \frac{1}{2} tr\left\{\frac{\partial R}{\partial\theta_i} R^{-1} \frac{\partial R}{\partial\theta_j} R^{-1}\right\} \tag{B.3}$$

Where *R* is the data covariance matrix given by $R = E\{xx^T\}$. The FI evaluation in (B.3) can be simplified if the matrix *R* is diagonal. This is achieved by replacing the data vector x by its Fourier coefficients, which are asymptotically uncorrelated.

Let $x(t)$ be a discrete time stationary zero-mean *n*-variate process with autocorrelation function $R(\tau) = E\{x(t)x^T(t+\tau)\}$. Its power spectrum density is defined as:

$$S(\omega) = \sum_{\tau=-\infty}^{\infty} R(\tau) e^{-j\omega\tau} \tag{B.4}$$

The elements of the Fisher Information from (B.3) can then be expressed as:

$$J_{ij} = \frac{T}{4\pi} \int_0^{2\pi} tr\left\{\frac{\partial S(\omega)}{\partial\theta_i} S^{-1}(\omega) \frac{\partial S(\omega)}{\partial\theta_j} S^{-1}(\omega)\right\} d\omega \tag{B.5}$$

This result also holds for a band-limited continuous time process which is sampled at the Nyquist rate.

For the case of time delay estimation, consider two noisy signals $r_1(t)$ and $r_2(t)$ which contain a common stationary process, $s(t)$, delayed in time.

$$\begin{aligned} r_1(t) &= s(t) + n_1(t) \\ r_2(t) &= s(t-D) + n_2(t) \end{aligned} \tag{B.6}$$

where $n_1(t)$ and $n_2(t)$ are uncorrelated additive noise processes. The relative delay, *D*, is estimated from measurements $\{r_1(t), r_2(t), 1 \le t \le T\}$. The Cramer-Rao bound for delay estimation error is formulated by first forming the spectral matrix of the vector process $[r_1(t), r_2(t)]^T$.

$$\mathbf{S}(\omega) = \begin{bmatrix} S(\omega) + N_1(\omega) & S(\omega)e^{j\omega D} \\ S(\omega)e^{-j\omega D} & S(\omega) + N_2(\omega) \end{bmatrix} \tag{B.7}$$

Then, upon differentiating the above expression with respect to the time delay parameter and performing the necessary matrix multiplications, the following is found:

$$\frac{\partial S(\omega)}{\partial D} S^{-1}(\omega) \frac{\partial S(\omega)}{\partial D} S^{-1}(\omega) = \frac{1}{|\mathbf{S}(\omega)|} \begin{bmatrix} \omega^2 S^2(\omega) & 0 \\ 0 & \omega^2 S^2(\omega) \end{bmatrix} \tag{B.8}$$

Where $|\mathbf{S}(\omega)|$ is the determinant of the spectral matrix $\mathbf{S}(\omega)$. When (B.8) is inserted into equation (B.5), the resulting expression for the Fisher Information is:

$$J(D) = \frac{T}{2\pi} \int_0^{2\pi} \frac{\omega^2 (S(\omega)/N_1(\omega))(S(\omega)/N_2(\omega))}{1 + (S(\omega)/N_1(\omega)) + (S(\omega)/N_2(\omega))} d\omega \tag{B.9}$$

From equation (B.9) we can see that the quadratic weighting in the Fisher Information arises as a result of differentiating $S(\omega)$ with respect to the time delay parameter, *D*.

B.2 The effects of carrier phase synchronization on the estimation process

This appendix demonstrates the effects of synchronization errors (between the local oscillator and the received carrier) on the TDOA/FDOA estimation process. Given two complex baseband signals with a common component shifted in frequency and time:

$$\begin{aligned} x_1(t) &= s(t)e^{j2\pi f_1 t} \\ x_2(t) &= s(t-D)e^{j2\pi f_2 (t-D)} \end{aligned} \tag{B.10}$$

The TDOA/FDOA estimation process is defined as:

$$\max_{\tau,f}\left|\int_0^T x_1(t)x_2^*(t+\tau)e^{-j2\pi ft}dt\right| \tag{B.11}$$

or equivalently:

$$\max_{\tau,f}\left|\int_0^T s(t)e^{j2\pi f_1 t}s^*(t+\tau-D)e^{j2\pi f_2(t-D)}e^{-j2\pi ft}dt\right| \tag{B.12}$$

Assuming that the signal is demodulated without the use of carrier phase synchronization, then let the phase offset at sensor *i* be θ_i. The baseband representations of the received signals at the two sensors are now:

$$\begin{aligned} x_1(t) &= s(t)e^{j(2\pi f_1 t+\theta_1)} \\ x_2(t) &= s(t-D)e^{j(2\pi f_2(t-D)+\theta_2)} \end{aligned} \tag{B.13}$$

The TDOA/FDOA estimation process requires searching over the magnitude of the modulated cross-correlation:

$$\left|\int_0^T s(t)e^{j(2\pi f_1 t+\theta_1)}s^*(t+\tau-D)e^{-j(2\pi f_2(t-D)+\theta_2)}e^{-j2\pi ft}dt\right| \tag{B.14}$$

$$=\left|e^{j(\theta_1-\theta_2)}\int_0^T s(t)e^{j2\pi f_1 t}s^*(t+\tau-D)e^{-j2\pi f_2(t-D)}e^{-j2\pi ft}dt\right| \tag{B.15}$$

$$=\left|e^{j(\theta_1-\theta_2)}\right|\left|\int_0^T s(t)e^{j2\pi f_1 t}s^*(t+\tau-D)e^{-j2\pi f_2(t-D)}e^{-j2\pi ft}dt\right| \tag{B.16}$$

$$=\left|\int_0^T s(t)e^{j2\pi f_1 t}s^*(t+\tau-D)e^{-j2\pi f_2(t-D)}e^{-j2\pi ft}dt\right| \tag{B.17}$$

Therefore, TDOA/FDOA parameter estimation does not require the use of a coherent phase reference when removing the carrier component from the observed signal. While an accurate phase reference is necessary for symbol detection, it has no effect on the TDOA/FDOA estimation process.

Appendix C: Experimental Setup

C.1 Preliminaries

The experiments performed in this thesis require the use of the MATLAB core, Communications Toolbox, and Signal Processing Toolbox. The following m-files were used in the simulations.

crMsg.m, tdoa.m, codec.m, bitalloc.m, bitallocfi.m, addnoise.m, Tx_symbols.m

C.2 Decimation Simulations

This simulation decimates and interpolates digital linearly modulated signals of different symbol rates, generating 100 random messages for each specified symbol rate. Decimation and subsequent interpolation are performed for multiple factors. The TDOA parameter is then estimated using both the compressed and uncompressed messages. The results for each message will be saved in the directory specified by *dec_path*.

```
%test effects of downsampling (varying symbol rate and decimation factor)
%Preliminaries:
%   msgR - message parameter structure
%   P,u - sensor/emitter coordinates
%   cdcP - codec parameter structure
%Experimental results:
%   td - matrix containing TDOA estimates obtained from uncompressed signals
%   ctd - TDOA estimates obtained from compressed signals

dec_path='results/dec/';            %path in which results are saved
M=[2:2:32 35 36 40 42 45 48];       %interpolation factors
F=[2 2 3:5 4 7 4 6 5 11 6 13 7 6 8 7 6 8 7 9 8];      %decimation factors
F=[F; 1 2 2 2 2 3 2 4 3 4 2 4 2 4 5 4 5 6 5 6 5 6];   %(two stages)
N_sym=256:256:12800;                %number of symbols
R_sym=(50:50:2500)*1000;            %symbol rates

for e=1:length(R_sym),              %for each symbol rate
msgR.R_sym=R_sym(e);
msgR.N_sym=N_sym(e);
msgR.x=[];                          %clear symbol vector

clear rtd ctd td
for k=1:100,                        %repeat 100 times
[msgk msgP]=crMsg(u,P,msgR,[]);     %create new message

msgkc=msgk;                         %copy other stuff over
for j=1:length(M),                  %for each decimation factor
    for i=1:(size(msgk,1)-1),
        K=length(msgk{i,1});
        Pad=ceil(K/M(j))*M(j)-K;    %calculate pad
        x=[msgk{i,1}; zeros(Pad,1)]; %zero-pad signal
        %decimate and interpolate
msgkc{i,1}=interp(decimate(decimate(x,F(1,j),'FIR'),F(2,j),'FIR'),M(j));
        msgkc{i,1}=msgkc{i,1}(1:end-Pad); %remove pad
```

```
    end
    ctd(j,:,k)=tdoa(msgkc,msgP,1);  %compressed TDOA estimate
    [td(j,:,k) rtd(j,:,k)]=tdoa(msgk,msgP,1); %uncompressed TDOA estimate
    %display status
    disp([num2str(M(j)) ': ' num2str(ctd(j,:,k)-td(j,:,k))]);
end
save([dec_path num2str(e)],'ctd','td','M','msgP');    %save results
end
end
```

C.3 Subband Encoding Simulations

This simulation will generate 100 random messages and perform subband encoding using MSE and FI-based distortion criteria. A bit allocation will be computed for each intercepted signal. The TDOA parameter is estimated using signals produced by both compression methods. The results are saved to the file *sub_file*.

```
%test FI vs MSE bitalloc with additive noise (varying SNR)
%Preliminaries:
%   msgR - message parameter structure
%   P,u - sensor/emitter coordinates
%   cdcP - codec parameter structure
%Experimental results:
%   td - matrix containing TDOA estimates obtained from uncompressed signals
%   ftd – TDOA estimates for signals compressed using FI criteria
%   mtd – TDOA estimates for signals compressed using MSE criteria
%   bf – subband bit allocations using FI criteria
%   bm – subband bit allocations using MSE criteria

clear td ftd mtd bm bf
sub_file='results/subband/experiment1';
N=fliplr([0:5:40]); %SNR

for i=1:100,                                %repeat 100 times
[msgb msgP]=crMsg(u,P,msgR,[]);             %create new message
for j=1:length(N),                          %for each SNR
    cdcP.n=max(abs(msgb{1,1}))^2/10^(N(j)/10);  %noise variance
    msgk=addnoise(msgb,N(j),N(j));          %add noise (WGN)
    cdcP.op='MSE';                          %change mode to MSE
    [msgkc bm(i,j,:,:)]=codec(msgk,cdcP); %compress using MSE alloc
    msgkc{3,1}=msgk{3,1};                   %dont compress signal 3
    mtd(i,:,j)=tdoa(msgb,msgP,1)-tdoa(msgkc,msgP,1); %MSE TDOA estimates
    cdcP.op='FI';                           %change mode to FI
    [msgkc bf(i,j,:,:)]=codec(msgk,cdcP); %compress using FI alloc
    msgkc{3,1}=msgk{3,1};                   %dont compress signal 3
    ftd(i,:,j)=tdoa(msgb,msgP,1)-tdoa(msgkc,msgP,1); %FI TDOA estimates

    td(i,:,j)=tdoa(msgb,msgP,1)-tdoa(msgk,msgP,1); %no-comp TDOA estimates
    disp(['MSE: ' num2str(mtd(i,:,j)) ' FI: ' num2str(ftd(i,:,j)) ' NO: '
num2str(td(i,:,j))]);                       %display status
end
save(sub_file,'ftd','mtd','td','msgP','bm','bf');     %save results
end
```

This simulation will generate 100 random messages and perform subband encoding using MSE and FI-based distortion criteria; however, unlike in the previous experiment, the bit allocation will be computed only once using a randomly generated message. This simulation generates the results for the suboptimal approach that was presented in section 4.3.

```
%test FI vs MSE bitalloc with additive noise (varying SNR, one-time alloc)
%   msgR - message parameter structure
%   P,u - sensor/emitter coordinates
%   cdcP - codec parameter structure
%Experimental results:
%   td - matrix containing TDOA estimates obtained from uncompressed signals
%   ftd – TDOA estimates for signals compressed using FI criteria
%   mtd – TDOA estimates for signals compressed using MSE criteria
%   bf – subband bit allocations using FI criteria
%   bm – subband bit allocations using MSE criteria

clear td ftd mtd
sub_file='results/subband/experiment1';
N=fliplr([0:5:40]); %SNR

[msgb msgP]=crMsg(u,P,msgR,[]);           %create message for bit alloc
for j=1:length(N),                        %for each SNR
    cdcP.n=max(abs(msgb{1,1}))^2/10^(N(j)/10); %noise variance
    msgk=addnoise(msgb,N(j),N(j));        %add noise (WGN)
    cdcP.op='MSE';                        %change mode to MSE
    [msgkc bm(j,:,:)]=codec(msgk,cdcP);   %compress using MSE alloc
    cdcP.op='FI';                         %change mode to FI
    [msgkc bf(j,:,:)]=codec(msgk,cdcP);   %compress using FI alloc
end

cdcP.op=[];
for i=1:100,                              %repeat 100 times
[msgb msgP]=crMsg(u,P,msgR,[]);           %create new message
for j=1:length(N),                        %for each SNR
    msgk=addnoise(msgb,N(j),N(j));        %add noise (WGN)
    cdcP.b=squeeze(bm(j,1,:));            %load MSE bit allocation
    msgkc=codec(msgk,cdcP);               %compress using MSE alloc
    msgkc{3,1}=msgk{3,1};                 %dont compress signal 3
    mtd(i,:,j)=tdoa(msgb,msgP,1)-tdoa(msgkc,msgP,1); %MSE TDOA estimates
    cdcP.b=squeeze(bf(j,1,:));            %load FI bit allocation
    msgkc=codec(msgk,cdcP);               %compress using FI alloc
    msgkc{3,1}=msgk{3,1};                 %dont compress signal 3
    ftd(i,:,j)=tdoa(msgb,msgP,1)-tdoa(msgkc,msgP,1); %FI TDOA estimates
    td(i,:,j)=tdoa(msgb,msgP,1)-tdoa(msgk,msgP,1); %no-comp TDOA estimates
    disp(['MSE: ' num2str(mtd(i,:,j)) ' FI: ' num2str(ftd(i,:,j)) ' NO: '
num2str(td(i,:,j))]);         %display status
end
save(sub_file,'ftd','mtd','td','msgP','bm','bf');     %save results
end
```

Vita

William W. Perkins was born on September 23, 1983, in New Orleans, Louisiana. After finishing high school in 2001, William moved to the nearby town of Baton Rouge to pursue an education in electrical engineering. He received his baccalaureate degree in electrical engineering in May 2005, then returned home to New Orleans. After losing his home to Hurricane Katrrina in August 2005, William evacuated to Baton Rouge, where he subsequently enrolled in the master's program in the Department of Electrical and Computer Engineering at LSU. William is expected received his Master of Science in Electrical Engineering degree with a specialization in communications and digital signal processing in August 2007. William plans to pursue a PhD in Communications Engineering at a university that is yet to be determined, beginning Fall 2008.